WCRP REPORT
World Climate Research Programme

Assessment of Global Precipitation Products

A project of the World Climate Research Programme Global Energy and Water Cycle Experiment (GEWEX) Radiation Panel

Lead Authors:

Arnold Gruber
Cooperative Institute for Climate Studies, Earth System Science Interdisciplinary Center, University of Maryland, College Park, Maryland

and

Vincenzo Levizzani
Institute of Atmospheric Sciences and Climate, Italian National Research Council, Bologna, Italy

May 2008

WCRP-128
WMO/TD-No. 1430

Table of Contents

Foreword
Preface
Executive summary
Chapter 1. Introduction 1
Chapter 2. Global Precipitation Data Sets 2
2.1 Introduction 2
2.2 GPCP monthly mean precipitation products 4
2.2.1 Input data and characteristics 5
2.2.1.1 Gauges 5
2.2.1.2 Satellite estimates 5
2.2.2 Analysis procedures 7
2.2.3 GPCP product error characteristics 9
2.3 Other precipitation data sets 10
2.3.1 CMAP 10
2.3.2 Passive microwave algorithms 11
2.3.3 TRMM-based microwave algorithms 12
2.3.4 Gauge Analyses 13
2.3.4.1 GPCC Products 13
2.3.4.2 GHCN+CAMS 13
2.3.4.3 Climate Research Unit 14
2.4 Chapter summary 14
Chapter 3. Spatial and Temporal Variability of Global Precipitation 15
3.1 Introduction 15
3.2 Global Mean Precipitation and Its Distribution 15
3.2.1 The Global Mean Precipitation Rate 15
3.2.2 The Global Distribution of Mean Precipitation 17
3.3 Mean Annual Cycle 19
3.3.1 Total, land-only and ocean-only mean annual cycle of precipitation 19
3.3.2 Annual Cycle of zonally averaged precipitation 19
3.3.3 Seasonal Evolution of Mean Precipitation Patterns 20
3.4 Seasonal-to-Interannual Variability 25
3.4.1 Time series of global monthly anomalies 25
3.4.2 Time series of zonal mean anomalies 28
3.5 Low Frequency Variations and Trends 28
3.6 Summary and Concluding Remarks 31
Chapter 4. Future outlook 33
4.1 Introduction 33
4.2 Improvements to the global data set 33
4.2.1 Observations 33
4.3 Future Measurements from Space 34
4.3.1 Global Precipitation Mission 34
4.3.2 The GPM Precipitation-Measuring Instruments 35
4.3.2.1 GPM Microwave Imager (GMI) 35
4.3.2.2 GPM Dual Frequency Radar (DFR) 36
4.4 Concluding Remarks 36
References 37
Appendix I. Acronyms 43
Appendix II. Contributors 45
Appendix III. Satellite Missions 47

Assessment of Global Precipitation Products

A Project of the Global Energy and Water Cycle Experiment (GEWEX) Radiation Panel
GEWEX, World Climate Research Programme

Lead Authors:

Arnold Gruber
Cooperative Institute for Climate Studies, Earth System Science Interdisciplinary Center, University of Maryland, College Park, Maryland
and
Vincenzo Levizzani
Institute of Atmospheric Sciences and Climate, Italian National Research Council, Bologna, Italy

WCRP-128

WMO/TD-NO. 1430

Foreword

The World Climate Research Programme (WCRP) was established in 1980 to pursue two major scientific objectives: 1) determine the extent to which climate can be predicted and 2) determine the extent of human influence on the climate system. Progress achieved by the WCRP in understanding of the Earth's climate system variability and change makes it possible to assess its predictability at a number of time scales and start using this predictive knowledge for developing an increasing range of practical applications of direct relevance, benefit and value to society. Such applications are most awaited by the global community in the areas of mitigation of climate change and adaptation to it in major social and economic sectors (e.g. food security, energy and transport, environment and health, water resources, etc.).

WCRP has organized its research program through four major Projects, namely the Global Energy and Water Cycle Experiment (GEWEX), Climate Variability and Predictability (CLIVAR), Stratospheric Processes and their Role in Climate (SPARC), Climate and Cryosphere (CliC), and a set of interdisciplinary cross-cutting research projects. These projects use a combination of coordinated international field experiments together with long-term climate data records through active participation of scientists from around the world to understand the underlying key climate processes, and use the scientific knowledge gained to develop climate models that mimic the behavior of the Earth's climate system across a wide range of time and space. These models are then used to develop future climate scenarios to assess the benefits/risks of climate conditions for policy decisions, practical applications and risk management.

This report is a synthesis of the current state of knowledge in measurements of global precipitation, a major component of the global water and energy cycle that influences significantly the Earth's climate system, and in turn is affected by the climate system variability and change. It is a comprehensive assessment of the current global precipitation data records which have been assembled by combining observations from space-based and in situ measurements. These long-term records include observations over the land and oceans for a period of 25 years. The report describes in detail how these precipitation records are developed, the underlying assumptions in sampling and processing procedures, their spatial and temporal resolution, and the potential sources of errors and anomalies in these records.

It is by far the most complete assessment and documentation of global precipitation records for use in assessing climate projections; however, the record length is too short for analysis of climate trends. The report provides new and useful information about the distribution and variability of global precipitation particularly over the oceans. It offers some very useful insights and guidelines for improving the current records both through observations and processing, and to expand these records in the future to capture the full three dimensional structure of clouds and hydrometeors based on the emerging polarimetric and multi-frequency active/passive microwave sensors. It identifies a special need for improved observation of snow rates and precipitation in complex terrain. The report also highlights the unique capabilities and contributions that the Global Precipitation Measuring (GPM) constellation of satellites under development in the USA, Japan and Europe can make by providing routine updates of global precipitation over 80% of the Earth once every three hours, as early as next decade.

We extend our great appreciation and gratitude to the authors, contributors and reviewers of this report on behalf of the World Climate Research Programme (WCRP) team for the insight and very useful information they provide in this report.

Ghassem R. Asrar, Director, WCRP

Preface

The charge given by the GEWEX Radiation Panel (GRP) to the Precipitation Assessment Group was to evaluate the reliability of available, global, long-term precipitation data products in depicting the variations of precipitation at larger than weather scales with a special emphasis on the Global Precipitation Climatology Project (GPCP) product that is produced under the auspices of the GRP. The original goal of GPCP was to produce a new precipitation product employing satellite observations that was globally complete and could provide a quantitative description of regional precipitation variations on seasonal to interannual time scales. However, the continuation of GPCP has allowed for extension of the record to 25 years (now approaching 28 years), so that the question of longer term variations arises. Moreover, a stronger emphasis on precipitation processes at weather scales has begun with GPCP efforts to obtain useful precipitation measurements on diurnal to daily time scales. The GRP views this assessment as one step in progress towards more accurate measurements of precipitation and as part of preparations for a systematic improvement, revision and re-processing of the global precipitation products.

William Rossow, Chair, GEWEX Radiation Panel, 2001-2007

Executive Summary

This assessment was conducted by an international group of scientist who are experts in the measurement and analysis of precipitation using remote sensing techniques and in situ gauges. Although focused on the data set produced by the Global Precipitation Climatology Project, the assessment also reviewed the current state of the art of satellite techniques for estimating precipitation as well as the variety of long term gauge data sets. An interesting aspect is that the satellite techniques discussed include single sensor (e.g., infrared, microwave) as well as multi spectral techniques, and time scales less than monthly and space scales finer than 2.5 × 2.5 degrees latitude/longitude. Clearly these retrieval algorithms are continuously evolving and we need to emphasize that the GPCP, which for the most part utilizes single sensor techniques that are decades old, will at some point have to consider the impact of new retrieval algorithms as well as sensors (e.g. Tropical Rainfall Measuring Mission, TRMM). ***This was suggested in Chapter 4 which called for a re-analysis where new retrieval techniques and sensors would be evaluated for use in global precipitation estimates along with higher space and time resolution data.***

Chapter 3 provides a review of the global mean precipitation and its spatial and temporal distribution. The analysis is based on the 25 year period 1979-2004, which exhibited a global mean of 2.61 mm day^{-1}. With regard to this value the authors of Chapter 3 provide an estimate of the uncertainty of ± .03 mm day^{-1}. They point out that at this level of uncertainty there is no significant mean annual cycle in global precipitation. This is consistent with global energy arguments that to a first approximation global precipitation should be more or less constant over the 25 year period. The mean annual cycle over the oceans and land are examined separately with the land areas showing the largest annual variation. Analysis of the spatial and temporal distribution of precipitation demonstrated that this data set is very capable in capturing the ENSO, the major interannual variation in precipitation, most evident in the tropics but also influencing mid-latitude regions. However, no relationship was found between global precipitation anomalies and ENSO.

The situation is not as clear with regard to longer period variations, especially since as noted in Chapter 3 that this data set was not designed for trend analysis. Also, as noted in Chapter 3 the analysis indicated that there was no discernable trend in global averaged precipitation. However, this does not preclude the existence of regional trends. Analyses were presented that indicate small areas of linear trend over land and the Indian and central to eastern Pacific Oceans. However, these data seem to suggest that the rainfall shifts between the 1982/83 and 1997/98 ENSO. A similar result was obtained using an Empirical Orthogonal Function (EOF) analysis which isolated the ENSO regime (modes 1 and 2) from the lower frequency variations (mode 3). Also, a recent analysis suggested that there were positive trends in the frequency of upper and lower amounts of precipitation but compensated by a negative trend in the frequency of intermediate amounts. Nevertheless, these trend calculations are very sensitive to the length of record and it was felt that with an increase in the GPCP record length questions concerning longer period variability and trends can be answered with greater confidence.

Based on the analysis presented in Chapter 3 we feel that it is crucial to continue this data set. It is clearly useful for studying inter-annual variability and increasing the length of record would help increase the reliability in the estimates of low frequency changes calculated on a regional scale. This would meet the requirements for applications of the data set to global climate analysis.

Chapter 4 provides a brief glimpse into the future. Given the increase of new satellite retrieval algorithms and other gauge data sets it seems reasonable to anticipate that a re-analysis of the GPCP would take place that would be able to demonstrate an improved accuracy of the global precipitation. ***One useful effort in particular would be to try and utilize the TRMM precipitation***

radar data to provide an oceanic reference for ocean precipitation in a similar way that gauges provide for the land areas.

Also identified was the need to determine snow fall rate using remotely sensed data and accurate precipitation in complex terrain, the latter being a problem for remote sensing techniques and gauges. Another possibility in the future is the application of data assimilation methods to observed and modeled precipitation in order to obtain a dynamically, physically and hydrologically consistent field of precipitation. This would require a collaborative research effort among data producers and modelers.

This chapter also identifies the international effort to obtain higher spatial and temporal resolution precipitation data through the Program to Evaluate High Resolution Precipitation Products (PEHRPP, http://essic.umd.edu/~msapiano/PEHRPP) Project. The creation of datasets in this direction will significantly enhance the usefulness of precipitation data from satellite sensors for regional climate analysis, which is a rapidly growing research area.

Finally the most significant future development for global precipitation is the Global Precipitation Mission (GPM). Briefly, this will be a satellite mission that will consist of a core satellite with an advanced dual-frequency precipitation radar and microwave instruments and a constellation of polar orbiting satellites whose precipitation estimates can be calibrated against those of the core satellite. It will extend the TRMM mission by providing coverage at higher latitudes at 3 hour intervals over nearly the entire globe**.** ***Clearly a challenge facing the global precipitation community is to develop methodologies for utilizing these new observations to improve and extend existing data sets such as GPCP thus providing long time records for assessing climate change signals.***

Chapter 1. Introduction

There are only a limited number of global precipitation data sets available for study of the global water cycle and its climatic variations as, for example, called for by the Integrated Global Observing Strategy Water Cycle Observations Theme (2000, approved in 2003). A widely available set of global precipitation data is the one produced by GPCP (Huffman et al. 1997; Adler et al. 2003). Although comparisons of this data set have been done with other global precipitation data (Gruber et al. 2000; Yin et al. 2004) it has not been independently and thoroughly assessed in terms of how reliable it is in representing temporal and spatial variations of precipitation for climate change and water cycle studies. This is crucial since a variety of satellite estimates of precipitation are employed in this data set as well as new methodologies for merging the satellite and gauge data.

At a planning workshop held in August 2004 at the Cooperative Institute for Climate Studies, University of Maryland it was decided to focus such an assessment on GPCP monthly mean data set (Huffman et al. 1997; Adler et al. 2003) with inclusion of other data sets as necessary. GPCP is an international effort initiated in 1986 as a project of the World Climate Research Programme (WCRP 1986) and it enjoys broad community support, one of the reasons for selecting this data set for assessment. Subsequently, the GPCP was incorporated into the Radiation Panel of the Global Energy and Water Cycle Experiment (GEWEX) of the WCRP. It was formed to improve understanding of seasonal to inter-annual and longer term variability of the global hydrological cycle, determine the atmospheric latent heating rates needed for weather and climate prediction models, and provide an observational data set for model validation and initialization and other hydrological applications. Its initial goal was to produce a ten year climatology of monthly global precipitation on a 2.5 º × 2.5 º latitude/longitude grid. In recognition of the vast areas of the globe that are not sampled by gauges it was clear that the project would rely heavily on satellite estimates of precipitation which would be merged with rain gauges where available. The early years of the project were spent in organizing the various components of the project (Xie and Arkin 1994) and going through the process of evaluating and selecting algorithms for the retrieval of precipitation from geostationary and polar orbiting satellites using visible (VIS)-infrared (IR) and PMW observations (Xie and Arkin 1994; Ebert et al. 1996). The first version of the GPCP merged satellite and gauge data set was produced in 1997 (Huffman et al. 1997). This version revealed a markedly different view of global precipitation, especially over the oceans, than previously depicted by other climatologies that did not have the benefit of satellite observations (e.g., Jäger 1976; Legates and Wilmott 1990). The initial success of the project led to an extension of the precipitation data set back in time to 1979 (Adler et al. 2003) providing a record of global monthly precipitation of 27 years long and continuing. Given the length of the GPCP climatology and its global coverage this data set is ideally suited for studying the global water cycle and has the potential for detecting a precipitation based global climate change signal.

This assessment reviews the procedures and input data used to produce the GPCP data set, its spatial and temporal variability, the future outlook for new and improved data sets, and recommendations about the quality and use of these data for studying the climate. While the assessment will focus on the GPCP data set, other sources of global precipitation data will be included as needed to help support the analyses and conclusions of this assessment.

Chapter 2. Global Precipitation Data Sets

2.1 Introduction

There is a pressing requirement for adequate observation and estimation of precipitation on a global scale stemming primarily from the paucity of such information over the vast majority of the Earth's surface. Conventional precipitation data sets, collected by gauges and, more recently, radar, suffer from spatial heterogeneity which given the temporal and spatial variability of precipitation leads to problems concerning the representativeness of the existing measurements.

Historically, precipitation has been measured in collection vessels such as the rain gauge (primarily for liquid precipitation) or snow gauges (for frozen precipitation). Such gauges provide the basis of long-term precipitation data sets and are generally deemed to be representative of the precipitation at the point of measurement. However, a number of factors affect the accuracy of such gauge measurements, such as gauge design, precipitation phase (liquid or solid), wind effects, evaporation/condensation, etc. Furthermore, gauges do not provide a reliable spatial measurement of precipitation. The global distribution of gauges is quite variable ranging from relatively dense gauge networks in the more developed countries to sparsely distributed gauges in less developed regions. Over the oceans gauges are essentially non-existent, with only a few gauges located on islands and atolls. The representativeness of the gauges is therefore extremely important: a 'good' gauge density of 20 gauges per 1×1 degree latitude/longitude box implies one gauge per area of 500 km^2. The vast majority of the globe has much poorer sampling. Surface morphology (relief, vegetation, etc) over land and island locations over the ocean lead to significant spatial inhomogeneity in the distribution of precipitation. Furthermore, heterogeneities arise from the characteristics of precipitation: convective precipitation tends to be localized and of short duration, making its measurement more difficult, while stratiform precipitation is typically larger-scale and longer-term. However, precipitation totals observed at neighboring stations usually have part of their variance in common depending upon season and region. At monthly time-scales even stations which are separated by hundreds of kilometers have on average about 50% of their precipitation variability in common.

The development of radar systems to measure precipitation has addressed some of the short-comings of the gauge data sets. First, radar is capable of providing a spatial measurement of precipitation (up to a certain distance from the radar location, typically about 100 km) and, second, it can provide frequent samples. Radar does however have a number of disadvantages. The conversion of the signal backscatter into rain-rates is not exact; surface effects and melting precipitation lead to anomalous signals, and low-level precipitation may be missed due to the upward-refraction of the radar beam through the atmosphere. Other issues include attenuation, beam blockage, beam-filling, and beam overshoot (e.g., Sauvageot 1994). Radar networks can however be usefully employed with cross-calibration and calibration from gauge data, although in terms of global coverage, radars generally cover regions that already have adequate gauge networks. The most useful application of radar in the generation of global precipitation datasets has probably been in the calibration and validation of satellite precipitation algorithms.

The estimation of precipitation on a global scale is therefore only viable through the utilization of Earth observation satellites. The first meteorological satellite was launched in 1960 and since then a plethora of sensors have been developed and launched to observe the atmosphere. These sensors fall into two main categories: VIS/IR sensors available from geostationary (GEO) and low-Earth orbiting (LEO) satellites and microwave sensors, currently only available from LEO satellites. The suite of geostationary satellites is able to continuously monitor the Earth, providing data up to every 15 minutes in operational mode. Meanwhile, the LEO satellites are capable of providing higher resolution data in the VIS and IR spectra, but only periodically when the satellites are passing overhead. Passive microwave (PMW) data, collected from LEO, has much poorer spatial resolution than the VIS/IR measurements coupled with poorer temporal sampling associated with LEO observations. Figure 2.1 and Table 2.1 provide an outline of the key satellites currently utilized for the retrieval of precipitation.

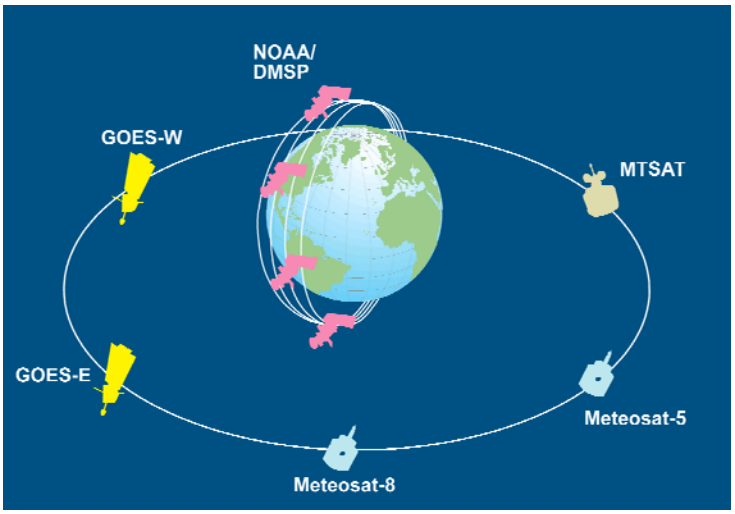

FIGURE 2.1: Distribution of satellites and their orbits used for GPCP precipitation retrieval.

TABLE 2.1: Summary of key satellites and sensors currently employed by mainstream precipitation algorithms.

Low Earth orbiting satellites

Satellite	Sensor	Spectral range	Channels	Resolution
NOAA 10/11/12	AVHRR	Vis & IR	5	1.1 km
	AMSU A & B	PMW	15/5	50 km (best)
	TOVS (HIRS/MSU/SSU)	Sounder		
DMSP F-13/14/15/16	SSM/I & SSM/IS	PMW	7 &	
TRMM	TMI	PMW	9	5-50 km
	PR	Radar	1	4.3 km

Geostationary satellites

Satellite	Sensor	Spectral range	Channels	Resolution
GOES E/W	GOES I-M Imager	Vis & IR	5	1 & 4 km
Meteosat 5,7,8	MVIRI & SEVIRI	Vis & IR	3 & 12	1 & 4 km
MTSAT		Vis & IR	5	1 & 4 km

A range of algorithms and techniques has evolved to provide estimates of precipitation from the data collected by these sensors. Estimates of precipitation derived from VIS/IR data sets rely upon the characteristics of the cloud tops: reflected VIS radiation can be used to infer the cloud thickness and height, while emitted thermal IR radiation is used to measure the temperature of the cloud tops. Since all precipitation falls from clouds, the delineation of clouds themselves can provide a crude map of precipitation. Algorithms such as the Geostationary Operational Environmental Satellite (GOES) Precipitation Index (GPI) described by Arkin and Meisner (1987) have shown that, despite their simplicity, over large space and time scales such techniques work reasonably well. The availability of geostationary data at relatively high spatial and temporal scales permits the evolution of clouds systems to be studied and precipitation estimates to be generated. Techniques such as the Griffith-Woodley technique (Griffith et al. 1978) and the convective-stratiform technique (CST, Adler and Negri 1987) exploit such data. Operational techniques such as the Interactive Flash Flood Analyzer (IFFA, Scofield 1987) and subsequently the Autoestimator (Vicente et al. 1998, 2002) have been implemented to provide estimates of precipitation in real-time for a number of applications. More recently, neural network techniques have been applied to these data sets like the Precipitation Estimation from Remotely Sensed Information using Artificial Neural Networks (PERSIANN) (Sorooshian et al. 2000).

The primary drawback of the VIS/IR techniques is that the observations only relate to the characteristics of the cloud tops, rather than the precipitation reaching the surface. In the mid-1970s work on identifying precipitation from PMW observations showed much promise (e.g., Savage and Weinman 1975; Weinman and Guetter 1977). Observations at microwave frequencies relate to the amount of water within the vertical column of the atmosphere being observed. At frequencies below 40 GHz the precipitation signal is primarily due to the emission of radiation from precipitation-sized particles, adding to the upwelling radiation stream from the surface. Above 40 GHz these particles start to scatter the upwelling surface radiation resulting in a reduction in the sensor-received radiation. The former (emission) characteristics are best viewed over a radiometrically cold surface, such as over bodies of water, whilst the latter (scattering) are best seen over radiometrically warm surfaces, such as the land surfaces.

Many PMW techniques now exist for estimating rainfall, ranging from the relatively simple, empirically derived and calibrated techniques (e.g., Ferraro 1997), through to those that use complex atmospheric physics and radiative transfer equations to derive estimates of precipitation (Kummerow et al. 2001). Comparisons between VIS/IR techniques and PMW techniques have shown that the PMW technique provides much better instantaneous estimates of precipitation (Ebert et al. 1996). This is primarily due to the more direct nature of the observations. However, for longer-term estimates, the VIS/IR techniques based on geosynchronous data tend to perform better due to their better temporal sampling.

The combination of both the PMW observations and the VIS/IR observations has therefore been the subject of much work in recent years. Adler et al. (1994) used PMW estimates to calibrate the IR precipitation estimates on large spatial and temporal scales. More recently techniques to generate PMW calibrated estimates at high resolutions (on the order of 10 km / 30 minutes) have been devised (e.g., Turk et al. 2000; Kidd et al. 2003; Joyce et al. 2004; Huffman et al. 2006). However, these techniques have yet to reach maturity and long time series of global precipitation estimates from these algorithms are not yet available.

2.2 GPCP monthly mean precipitation products

The GPCP is a mature global precipitation product that uses multiple sources of observations, including surface information. Huffman et al. (1995, 1997) describe the GPCP product generating estimates at the 2.5 × 2.5 degree monthly resolution, this resolution being later improved to 1 × 1

degree daily estimates (Huffman et al. 2001) and 2.5 × 2.5 degree pentad estimates (Xie et al. 2003). The current GPCP Version 2 Satellite-Gauge (SG) product is described here.

One of the major goals of the GPCP is to develop global precipitation analyses at monthly and finer time scales to permit a more complete understanding of the spatial and temporal patterns of global precipitation. The merging of estimates from multiple sources takes advantage of the strengths offered by each type: local unbiased estimates where rain gauge data are available, physically-based PMW rain rates estimated from LEO satellites, and high temporal resolution indirect estimates from VIS/IR sensors on GEO satellites. Data from over 6000 rain gauge stations together with satellite IR and PMW observations have been merged to estimate monthly rainfall on a 2.5 degree global grid from 1979 to the present. The GPCP's Global Precipitation Climatology Centre (GPCC) maintains a collection of high quality rain gauge measurements that are used to prepare comprehensive land-based rainfall analyses. The careful combination of satellite-based rainfall estimates provides the most complete analysis of rainfall available to date over the global oceans, and adds necessary spatial detail and bias reduction to the rainfall analyses over land. In addition to the combination of these data sets, careful examination of the uncertainties in the rainfall analysis is provided as part of the GPCP products.

2.2.1 Input data and characteristics

2.2.1.1 Gauges

For the period 1986 to the present the monthly gauge analyses are constructed by the GPCC operated by the German Weather Service. The GPCC uses a variant of the spherical-coordinate adaptation of Shepard's method (Willmott et al. 1985) to interpolate the data observed at gauge stations to regular grid points at a resolution of 0.5 × 0.5 degree. These regular points are then averaged to provide monthly precipitation totals at the final 2.5 × 2.5 degree resolution. This methodology helps counteract the uneven distribution of gauges in the final gauge product. The Version 2 rain gauge “monitoring” product is based on about 6500 to 7000 rain gauge stations worldwide, mostly synoptic and monthly climate reports collected from the Global Telecommunications System (GTS) in real time. This is supplemented by other worldwide data collections such as Monthly Climatic Data for the World when available. Sophisticated quality control is performed before carrying out the analyses. A general description of the GPCC data processing and analysis system is given by Rudolf (1993), the methods are described by Rudolf and Schneider (2005). Bias correction factors are applied to the Version 2 gauge product in order to compensate systematic gauge measuring errors (see section 2.2.3).

Prior to 1986 (January 1979-December 1985), a combination of rain gauge products from the Global Historical Climatology Network (GHCN) produced by the NOAA/National Climate Data Center, Ashville, North Carolina, USA and the Climate Assessment and Monitoring System (CAMS) produced by the CPC, NCEP and NOAA. The same analysis of the gauge data is undertaken as for the GPCC data described above (see also Xie et al. 1997), although with less stringent error checking, corrections for systematic errors, etc.

2.2.1.2 Satellite estimates

The mainstay of the current GPCP products are precipitation estimates derived from the PMW satellite data sets, having the main advantage of being more direct than VIS/IR techniques. However, due to the behavior of the surface background, the ocean and land regions are treated separately.

Oceanic rainfall accumulations and other rain rate parameters are derived from the Special Sensor Microwave/Imager (SSM/I) sensor at 5º × 5º and 2.5º × 2.5º resolutions by the GPCP-Polar Satellite Precipitation Data Center (PSPDC) located at NASA/GSFC (URL: http://gpcp-pspdc.gsfc.nasa.gov). The algorithm is based on a non-linear rain rate-brightness temperature (Tb) relationship derived from radiative transfer modeling of an atmospheric model that is specified by the rain intensity and the freezing height (height of the zero degree isotherm) (Wilheit et al. 1991). The freezing height acts as a proxy of the integrated columnar water vapor. A channel combination of the 19 and 21 GHz observations are used to minimize the effect of water vapor variability on the microwave rain signature. Monthly histograms of the channel combination are then fitted to a mixed lognormal rain rate distribution via the rain rate-Tb relationship (Kedem et al. 1990). A beam-filling correction is applied to the monthly rain rate to account for the bias introduced by the coupling between the inhomogeneity within the rain field and the non-linearity of the rain rate-Tb relationship. The beamfilling correction is dependent on rain rate variability within the sensor field of view and the freezing height (Chiu et al. 1990; Wang 1995). The functional dependence of the beamfilling correction on freezing height is based on model simulation using airborne radar observations. Sampling errors of the products are of the order of 10-15% and are estimated using different sampling strategies and comparison with TRMM Microwave Imager (TMI) sampling (Chang and Chiu 1998).

A separate global product is generated by NOAA/NESDIS, utilizing an 85 GHz scattering approach over land and coast, and a blended 85 GHz scattering and 19-37 GHz emission approach over ocean. The GPCP only uses the land and coastal (generated 25 km either side of the coastline) portions of the product. The land/coastal portion of the GPCP SSM/I precipitation algorithm originates from the work of Grody et al. (1991), further developed by Ferraro et al. (1994), Ferraro and Marks (1995), and Ferraro (1997). The algorithm has been empirically tuned with ground radar measurements (see Ferraro and Marks 1995). Failure of the SSM/I 85 GHz vertical channel on the DMSP F08 satellite from June 1990 to late 1991 necessitated the substitution of the primary scheme with one using the 37 GHz channels, resulting in a loss of sensitivity in the rain retrievals from 1 mm h^{-1} to 5 mm h^{-1}. This algorithm also serves as the current DMSP SSM/I operational precipitation retrieval that is supplied in the Environmental Data Records (EDRs) generated at the Fleet Numerical Meteorology and Oceanography Center (FNMOC).

IR data sets are used to augment the PMW data sets primarily due to their better temporal and spatial sampling. The geosynchronous IR-based estimates use the GPI cold-cloud duration technique for precipitation retrievals from 40°S – 40°N. Data generated from each of the cooperating satellite operators in the US, Japan and Europe are compiled into 3-hourly histograms of cloud top temperatures at a resolution of 2.5º × 2.5º for each pentad (5-day) period from 1986-1996. Starting in 1997 the spatial resolution was increased to 1º × 1º. Inter-satellite and viewing angle corrections are performed based upon the scheme of Joyce and Arkin (1997). Where data from the geostationary satellites is unavailable (i.e. over longitudes in the Indian region), data from the Advanced Very High Resolution Radiometer (AVHRR) on the NOAA LEO satellites is used. These data sets are then used to derive the GPI estimates based upon the fractional coverage of cloud colder than 235 K, multiplied by a mean conditional rain rate of 3 mm h^{-1}.

The version 2 of the GPCP precipitation product also utilizes estimates generated from the outgoing longwave radiation (OLR) Precipitation Index (OPI, Xie and Arkin 1998). Lower values of outgoing longwave radiation are indicative of deeper clouds and hence precipitation. By mapping the anomalies between the climatological and the observed values the total precipitation may be inferred. For GPCP purposes the OPI are calibrated against the globally complete GPCP estimates for 1988-1998, which provides the calibration of the OPI technique for the period from January 1979-June 1987 and December 1987.

TABLE 2.2: Summary of input data sets used in the GPCP Version 2 SG.

Algorithm	*Input data*	*Space scale*	*Time scale*	*Areal coverage*	*Time coverage*	*Data provider*
GPCC gauge analysis	~6500 surface stations	2.5°	Monthly	Global land	1986– present	DWD/GPCC
CAMS+GHCN gauge analysis	~6500 surface stations	2.5°	Monthly	Global land	1979– 1985	NOAA/CPC
Emission-based PMW estimates	SSM/I on DMSP F08, F11, F13	2.5°	Monthly	60°N– 60°S ocean	July 1987– present	NASA/GSFC Lab. for Atmos.
Scattering-based PMW estimates	SSM/I on DMSP F08, F11, F13	2.5°	Monthly	Global	July 1987– present	NESDIS/ORA
AGPI	all GEO and LEO IR T_b's	2.5°	Pentad	40°N– 40°S	1986– 1996	NOAA/CPC
		1°	3-hour	40°N– 40°S	1997– present	
TOVS-based estimates	TOVS sounding data	1°	Monthly	Global	July 1987– present	NASA/GSFC Lab. for Atmos.
OPI	LEO-IR	2.5°	Monthly	Global	1979– June 1987	NOAA/CPC

Despite the relatively high quality ascribed to PMW estimates, all current algorithms falter in cold-land, icy-surface, and polar conditions. To provide more complete coverage of satellite-based estimates, particularly in cold seasons and at high latitudes, data from the Television-Infrared Observation Satellite (TIROS) Operational Vertical Sounder (TOVS) instrument are employed. The TOVS instrument is carried on two NOAA polar orbiting LEO satellites and provides input to the GPCP product for July 1987-February 1999, and a single sensor from March 1999-present. Retrievals of precipitation from the TOVS instrument are based upon parameters that relate to cloud volume: cloud-top pressure, fractional cloud cover and relative humidity profiles. A model is used to provide an initial guess of the moisture field, that is then tuned further by the satellite retrievals. The resulting product is averaged to 1 × 1 degree, monthly resolution. The main purpose of the TOVS products is to provide data poleward of the 40 degree latitude boundary associated with the IR-region, and over cold surfaces that restrict the retrieval of precipitation from PMW observations.

2.2.2 Analysis procedures

The Mesoscale Applications and Processes group at NASA/GSFC have developed and computes the current GPCP Version 2 Satellite-Gauge (SG) data set based on a variety of input data sets provided by other GPCP components (see above and Table 2.2). When the Version 2 SG was designed, inputs were selected to provide a reasonable, stable base from the changing mix of quasi-global satellite and rain gauge information that has been recorded over the period of continuous satellite records related to precipitation, namely 1979 to the present. Highlights of the SG algorithm are summarized below for each major data epoch, drawing on the more detailed material in Adler et al. (2003). Although reasonable care has been taken to minimize discontinuities between the data epochs, possible statistical inhomogeneities can arise due to known changes in data coverage. Throughout the record, the GPCP SG algorithm applies the Legates (1987) climatological bias

correction to all gauge analyses to account for gauge exposure. The combination procedure is divided into two main periods: January 1979-June 1987 and July 1987-present.

1987-present: For most of the period of record, beginning in July 1987, but not including December 1987 due to operational considerations, the SG incorporates SSM/I PMW estimates. To avoid possible changes in bias due to shifts in the time-of-day of SSM/I observations, the GPCP SG only uses data from the early morning Defense Meteorological Satellite Program (DMSP) platforms (F08, F10-15). To draw on their perceived strengths, the SSM/I and TOVS estimates are composited as follows:

- SSM/I estimates are used without modification within the band 40°N-40°S.
- TOVS estimates are adjusted to the zonally averaged bias of the SSM/I data within the band 40°N-40°S and inserted in SSM/I data voids caused by snow and other cold surfaces.
- Just outside of the band 40°N-40°S, the SSM/I and TOVS data are averaged.
- Further towards the poles the SSM/I-TOVS average is replaced with bias-adjusted TOVS data. The bias adjustment varies linearly between the zonal average of the SSM/I-TOVS average on the equatorward side and the zonal average monthly climatological rain gauge analyses on the polar side.
- Above 70°N, TOVS data are bias-adjusted to the zonal average of the available monthly rain gauge data.

The IR brightness temperatures (IR Tb's) are corrected for zenith-angle viewing effects and inter-satellite calibration differences, and are converted into precipitation estimates by applying the adjusted GPI algorithm (AGPI, Adler et al. 1994) as follows. A month of approximately time/space matched IR Tb's and SSM/I rain estimates are collected on a global grid in the latitude band 40°N-40°S. For each grid box, the GPI rain/no-rain threshold of 235 K (Arkin and Meisner 1987) is applied, then all the "raining" subsetted IR pixels are used to compute a single conditional rain rate such that they sum to the total rain in the coincident subset of SSM/I pixels. This procedure is carried out separately for geostationary and low-Earth orbit IR data.

A weighted combination strategy is used to merge the rainfall estimates in regions where more than one type of estimate is produced. The weight assigned to each estimate is defined by the inverse of its error variance, described at the end of this section.

With all of the input data now in the form of monthly precipitation estimates on a 2.5° × 2.5° grid, the Multi-Satellite (MS) estimate is computed as:

- AGPI estimates where available (40°N-40°S),
- weighted combination of the merged SSM/I-TOVS estimates and the LEO-AGPI elsewhere in 40°N-40°S, and
- composited SSM/I-TOVS data outside of 40°N-40°S.

Finally, the SG product is produced in two steps:

- Over land the MS estimate is adjusted to the large-scale gauge average over 5x5 arrays of grid boxes.
- The gauge-adjusted MS estimate and the gauge analysis are combined in a weighted average.

1979-1987: The period before the start of SSM/I observations requires more approximate schemes. During the period 1986-June 1987, plus December 1987, OPI data are climatologically calibrated by the 1988-98 GPCP SG estimates and used in place of the SSM/I-TOVS component (above). The MS field is built from geo-AGPI estimates where available (40°N - 40°S) and calibrated OPI estimates elsewhere, then the combination with the gauges proceeds as in the 1987-present era to produce the SG. Since the GPCP summaries of GEO-IR data are not available during 1979-1985,

so the calibrated OPI data are used "as is" for the MS estimates, and the gauge combination proceeds as in the recent era to produce the SG.

Throughout the processing, an estimate of the random error is produced for each grid box in each input, intermediate, and output precipitation estimate field following Huffman (1997). A method to quantify both the algorithm and sampling errors associated with the Ferraro (1997) algorithm were developed by Li et al. (1998) and Ferraro and Li (2002). Additionally, Chang et al. (1993) explored the random errors associated with Wilheit et al. (1991) algorithm. For the most part, the errors described in these studies are captured by the Huffman (1997) scheme. Validation of the random error estimation scheme by Krajewski et al. (2000) demonstrated that the Huffman (1997) parameterization gives reasonably good estimates over a wide variety of conditions in the United States.

2.2.3 GPCP product error characteristics

Gridded rain gauge precipitation is subject to different kinds of errors. First, precipitation measurement using gauges are affected by systematic errors, primarily losses due to aerodynamic effects, especially with snow, and evaporation, especially with heated instruments or hot weather. This error is estimated based on instrument intercomparison studies summarized by Sevruk (1989), and compensated using bulk correction factors for monthly climatological conditions following Legates and Willmott (1990). Measurement errors are investigated and minimized by an automatic pre-control followed by a visual control of unclear cases. In addition to systematic and stochastic measuring errors there is a sampling error (due to poor station density) and a methodical error (due to the interpolation method). Intercomparison studies by GPCC revealed that the methodical error is much smaller than the sampling error. Details on the sampling error and availability of data are discussed by Rudolf et al. (1994, 1998). The sampling error dominates the total error of the Version 2 gauge product, especially for data poor regions and where precipitation is highly variable.

The GPCP SG validates relatively well against standard and special gauge data sets, in part because the gauge adjustment scheme prevents significant bias (Krajewski et al. 2000; Adler et al. 2003) and in part because the adjustment accounts for uncertainty in the gauge analysis. In general there is a decrease in accuracy as the precipitation becomes light, the environment becomes more polar, and/or the surface becomes icy or frozen.

Over oceans there is a general lack of gauge data, so the SG equals the MS product, and validation studies are quite limited. Validation against the Pacrain atoll rain gauge data (Morrissey et al. 1995) in the tropical Pacific Ocean tends to show a low bias of some 12%, which is traceable to the calibration by the Wilheit et al. (1991) estimates used in that region (Adler et al. 2003). For the latitude band 30°N-30°S the time series of estimated area-average precipitation over ocean from GPCP closely matches Version 6 estimates made with TMI data using the Goddard profiling Algorithm (GPROF), (Kummerow et al. 1996; Olson et al. 1999).

In regions of complex terrain the PMW estimates sometimes fail to capture orographic enhancements, and this shortcoming is propagated to the AGPI, MS, and SG products. Meanwhile the gauge analysis tends to underestimate the precipitation because relatively few gauges are located at the higher elevations, where the heavier precipitation occurs (Nijssen et al. 2001). This known problem is under study, but no corrective scheme has yet been developed.

An estimate of random error for the GPCP product is provided as part of the data set (Huffman et al, 1997). It is dependent on the mean rain rate and the number of independent samples such that the lower the rain rate the lower the error and the higher the number of samples the lower the error. Thus in areas where the rain rate is low, e.g. semi-arid areas and polar latitudes the random error is

small whereas in areas with average rain rates but with large sampling, e.g. mid-latitudes Europe and North America the random error is also small. Over the raining tropical oceans and mid-latitude storm tracks the errors are larger due to higher rain rates and lower number of samples (satellite sampling only). Figure 2.2 is an example of the error estimates for August 1987 along with the associated monthly mean precipitation.

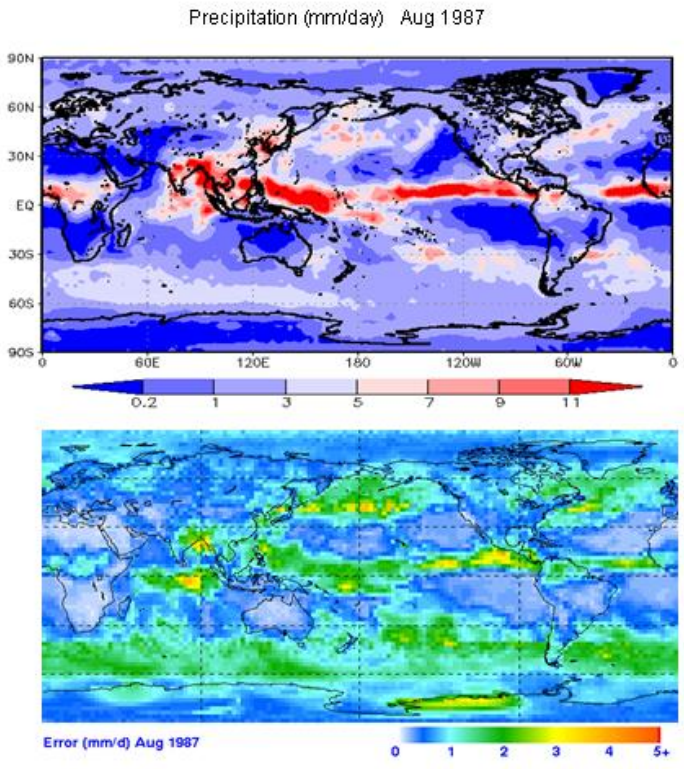

FIGURE 2.2: Satellite-gauge (SG) estimate of precipitation (top, in mm day^{-1}) and error estimate (bottom) for August 1987. (Error figure courtesy of G. Huffman and D. Bolvin)

These error characteristics were used in a study comparing GPCP with the NCEP NCAR reanalysis precipitation, (Janowiak et al. 1998).

2.3 Other precipitation data sets

This section provides a brief description of some other satellite and gauge data sets that have relatively long time series. TRMM is included in this discussion despite its relatively short length because of its importance as a possible reference data set for tropical rainfall.

2.3.1 CMAP

The Climate Prediction Center (CPC) Merged Analysis of Precipitation (CMAP), (Xie and Arkin 1997) produces pentad and monthly analyses of global precipitation in which observations from raingauges are merged with precipitation estimates from several IR and PMW satellite-based algorithms. The analyses are on a 2.5 × 2.5 degree latitude/longitude grid and extend back to 1979. These data are comparable to (but should not be confused with) the GPCP Version 2 monthly product described above.

It is important to note that the input data sources to make these analyses are not constant throughout the period of record. For example, SSM/I (PMW - scattering and emission) data became available in July of 1987; prior to that the only microwave-derived precipitation estimates available are from the MSU algorithm (Spencer 1993) which is emission-based and therefore available only over oceanic areas. GPCP eventually declined to use MSU because the time series exhibited undue sensitivity to the sea surface temperature, meaning there was an artificial correlation to ENSO (Xie, personal communication). Furthermore, archives of high temporal resolution IR data from geostationary satellites (every 3-hr) became available during 1986; prior to that, estimates from the OPI technique (Xie and Arkin 1997) are used based on OLR from polar orbiting satellites.

The merging technique is thoroughly described in Xie and Arkin (1997). Briefly, the methodology is a two-step process. First, the random error is reduced by linearly combining the satellite estimates using the maximum likelihood method, in which case the linear combination coefficients are inversely proportional to the square of the local random error of the individual data sources. Over global land areas the random error is defined for each time period and grid location by comparing the data source with the rain gauge analysis over the surrounding area. Over oceans, the random error is defined by comparing the data sources with the rain gauge observations over the Pacific atolls. Bias is reduced when the data sources are blended in the second step using the variational blending technique of Reynolds (1988). Here the data output from step 1 is used to define the "shape" of the precipitation field and the rain gauge data are used to constrain the amplitude, with the constraint that gauge analysis values are accepted “as is” for grid boxes at the edges of oceanic data voids and for grid boxes with 5 or more gauges.

Yin et al. (2005) have done an extensive comparison of CMAP with GPCP version 2, identifying a number of problems within both data sets. They concluded that the large scale precipitation fields are similar but that significant regional differences exist, such as an artificial trend in the tropics in the CMAP data set, a result of atoll data sampling deficiencies and the way they are used in the merging procedure.

2.3.2 Passive microwave algorithms

As previously described, a global SSM/I climatology has been produced by NOAA/NESDIS (Ferraro 1997) and is continuously updated on a monthly basis and exists for the time period July 1987 to present. The data are archived at the National Climatic Data Center (NCDC) and can be accessed at http://lwf.ncdc.noaa.gov/oa/satellite/ssmi/ssmiproducts.html.

Chang et al. (1993) developed a technique for the retrieval of monthly precipitation over the oceans between 50ºN and 50ºS at a resolution of 2.5º × 2.5º. The technique was designed to minimize the effect of water vapor on the precipitation retrievals by taking into account the height of the freezing level, as well as compensating for the inhomogeneity of the rainfall by providing a beam-filling correction. The estimates, when compared with the Pacific atoll gauge data set, showed low bias and good correlations.

GPROF is a multichannel physically-based algorithm for the retrieval of rainfall and vertical structure information from satellite-based PMW observations. The technique is described in Kummerow et al. (1996). An extensive library of vertical profiles is generated from a cloud resolving model to provide input to radiative transfer computations. A Bayesian inversion method is then applied to compare the observed microwave brightness temperatures with the model-based calculations to determine the most likely vertical profile. The GPROF scheme includes a procedure that accounts for inhomogeneities of the rainfall within the satellite field of view. Over ocean, convective/stratiform classification is performed, and convective rain rates are assigned in concentric rings, as described in Olson et al. (1999). Over land and coastal surface areas, the

algorithm employs extensive screening, then selects the most applicable of a limited number of hydrometeor profiles, using a scheme developed at NOAA (McCollum and Ferraro 2003, 2005).

An on-line data set derived from the GPROF scheme is available from the NASA/GSFC Distributed Active Archive Center. It currently contains a suite of nine products providing instantaneous gridded values of precipitation totals for each granule (orbit, or later, half-orbit) and supporting information for most of the SSM/I data over the roughly 18-year period July 1987 through present: http://lake.nascom.nasa.gov/data/dataset/TRMM/01_Data_Products/06_Ancillary/02_GPROF6/index.html. The products include precipitation estimates, pixel counts, two quality measures, column-integrated liquid and ice content, and an average time tag for each grid box, all based on the GPROF 6.0 physical retrieval algorithm, computed from SSM/I data. The main product, the surface rainfall, is the average surface rainfall rate in each 0.5 × 0.5 deg latitude/longitude grid box in hundredths of mm h^{-1}. A parameter is also provided that describes the average portion of the convective rainfall rate in each grid box.

More recently PMW observations from the Advanced Microwave Sounding Unit-B (AMSU-B) instrument have been converted to precipitation estimates at the National Environmental Satellite Data and Information Service (NESDIS) with operational versions of the Zhao and Weng (2002) and Weng et al. (2003) algorithm. It is most recently described in Ferraro et al. (2005) and Qiu et al. (2005). The Ice Water Path (IWP) is computed from the 89 and 150 GHz channels, with a surface screening that employs ancillary data. Precipitation rate is then computed based on the IWP and precipitation rate relationships derived from cloud model data computed with the NCAR/PSU Mesoscale Model Version 5 (MM5). The maximum precipitation rate allowed is 30 mm h^{-1}. The AMSU-B algorithm can discriminate between precipitating and non-precipitating ice-bearing clouds, but cannot provide information on precipitation systems that lack the ice phase. However the AMSU-B estimates have three issues. First, the AMSU is a cross-track scanning instrument, so pixel resolution and aspect vary with scan position. Second, the NESDIS algorithm was upgraded on 31 July 2003, yielding different bias and frequency of precipitation statistics before and after the change. Third, in both periods the AMSU-B has a pixel-level detectability limit of 1 mm h^{-1}. This causes the estimated fractional occurrence of precipitation to be low, critically so in the subtropical highs. Nonetheless, in regions of moderate and high precipitation experience shows that these estimates can be usefully employed. The algorithm developers are addressing these issues for future releases of the NESDIS algorithm. Finally, recent work indicates the potential for the detection of snowfall over land through the use of the sounding channels available on AMSU (Kongoli et al. 2003).

2.3.3 TRMM-based microwave algorithms

TRMM was successfully launched in November 1997 (Kummerow et al. 1998, 2000). Since then data over more than eight years have been accumulated. TRMM observations are focused on the rain over tropical and sub-tropical regions, with swaths extending to 38°N-38°S. TRMM is equipped with the first spaceborne precipitation radar (PR) along with a PMW radiometer (TMI) and a VIS/IR radiometer (VIRS). Those sensors observe precipitation system nearly simultaneously, which is unique and invaluable for rain retrieval algorithm development (Iguchi et al. 2000). Although the PR is a single wavelength radar with a relatively high frequency of 13.8 GHz, the so-called surface reference technique which utilizes the strong signature from the surface works well. This technique is peculiar to the downward-looking radar. The introduction of PR data opened a new field of radar rain estimation from space. This field will naturally extend to the future dual-wavelength radar algorithms planned, for example, for the GPM project's core satellite. The comparison of TMI-derived rainrate and PR-derived rainrate helped to improve rainfall estimates (e.g., Viltard et al. 2000; Prabhakara 2002). For example, the PR rain profiles highlighted a problem in the rain height assumption in the TMI algorithm (Masunaga et al. 2002; Ikai and

Nakamura 2003). Combination of PR and TMI data with the Lightning Imaging Sensor (LIS) has resulted in improved understanding of global precipitation systems. For example, rain systems over land are generally more vigorous than those over the ocean and may have more supercooled water (Nesbitt et al. 2000; Toracinta et al. 2002; Cecil et al. 2002).

Some comparisons of rain distributions derived by GPCP, TRMM and others have been done (e.g., Kodama and Tamaoki 2002), but it is not intensive. One obstacle is the retrieval of solid precipitation by the PR. For wet snowfall (i.e., the "bright band"), the equivalent rain rate estimates are inaccurate and should not be trusted.

2.3.4 Gauge Analyses

Gauge analyses suffer two primary quality issues, one being instrumental error and the other being analysis error. As discussed in sec. 2.2.3 nearly every gauge type underestimates precipitation due to aerodynamic effects, and these affect light and solid precipitation more severely than heavy rainfall. It is important to note that none of the precipitation products listed below have been corrected for gauge biases. Thus, regions where there is light precipitation (such as drizzle), or solid precipitation (i.e. snow) are likely to report values lower than the actual precipitation. Legates (1987) developed global monthly grids of climatological corrections that provide a first-cut estimate of the undercatch, and these have been applied in the GPCP products that incorporate gauge analyses.

2.3.4.1 GPCC Products

Aside from the monitoring product (see sec. 2.2.1.1) the GPCC offers three further global monthly precipitation products:

- The First Guess Product is based on automatically processed synoptic data received by GTS. Near real-time gridded monthly precipitation totals (1° grid) are supplied to individual users based on joint agreements.
- The Full Data Product includes the data base of the Monitoring Product as well as additional monthly precipitation data delivered by national agencies or other institutes of 173 countries. The number of available stations varies with time. Its maximum is about 40000 stations in 1987 but decreases monotonically afterwards. Globally gridded monthly precipitation totals are available for the period 1951 to 2004 from the GPCC Website (https://gpcc.dwd.de) or on email-request (gpcc@dwd.de).
- The Gridded Historical Precipitation Dataset is based on the merged data from GHCN, CRU, the Food and Agriculture Organization of the UN (FAO) and the GPCC database. Special attention is given to inhomogeneities and outliers. Only the homogenized and nearly gap-free time series of 9343 stations are taken into account. However, long term means of over 28000 stations are used in order to estimate average precipitation fields. Finally, relative anomalies for each month are interpolated. All interpolations are performed using ordinary kriging with local and seasonal de-correlation lengths estimated from the observations. A first version covering the period 1951 to 2000 is published (Beck et al. 2005). Data are available at the GPCC web site (see above).

2.3.4.2 GHCN+CAMS

GHCN processes a number of parameters to provide a comprehensive global surface baseline climate data set, of which precipitation is included. The data covers the period from 1697 to the (near-) present, although not all parameters are available over the full extent of this period. The precipitation data has been combined with the Climate Anomaly Monitoring System (CAMS to

produce the GHCN+CAMS data set, which is then used as an input to the GPCP monthly precipitation product.

2.3.4.3 Climate Research Unit

The CRU of the University of East Anglia (UK) have produced a 0.5 degree resolution data set of monthly surface-based climate parameters covering the period 1901-2002 (New et al. 2000; Mitchell and Jones 2005). Amongst these parameters monthly accumulations of precipitation are generated from available gauge data sets. Although the time series extends back to 1901, it should be noted that the number of available gauges varies with time: in 1901 4957 gauges contribute to the data set, peaking in 1981 with 14579 gauges. The CRU inserts synthetic zero anomaly values in regions that are "too far" from observations (i.e. farther than 450 km), while the other schemes simply interpolate over the entire distance.

2.4 Chapter summary

The measurement of precipitation for climate analysis is not straightforward. Precipitation is itself not homogenous in terms of its distribution in time and space. The continuity of precipitation records is not ideal, with many stations having fractured records, or records covering limited periods of time. Indeed, the "historical" records of precipitation are derived from land-based measurements and observations and therefore do not provide any information on precipitation over the majority of the Earth's surface – the oceans. Measurement of precipitation over the oceans using satellite observations is beginning to provide initial insights into changes of precipitation distribution and amounts. Although the record length of the satellite observations is still relatively short, these observations provide a starting point for investigating precipitation trends across the whole globe.

GPM mission has the primary aim of improving spatial and temporal sampling of precipitation, critical to the reduction of sampling errors currently inherent in estimates derived from low Earth orbit satellite observations. More importantly it provides a coordinated framework around which other precipitation measurements can be included for a more complete picture of global precipitation. It is interesting to note that PMW imaging sensors, despite being more direct that VIS and/or IR sensors for the retrieval of precipitation, are yet to be included in any operational platform. Although improvements in satellite observations of precipitation are sought, it should also be noted that gauge measurements provide the only long-term direct measure of precipitation and should not be overlooked.

Chapter 3. Spatial and Temporal Variability of Global Precipitation

3.1 Introduction

The GPCP data set spans over 25 years (Adler et al. 2003) and provides an opportunity to study global-scale precipitation in ways that were difficult to impossible before the start of this project. From the standpoint of climate variability studies the strengths of this data set are in its a) consistent data analysis, quality control, and data processing, b) an analysis of precipitation over both land and ocean and c) the use of a consistent set of global precipitation estimates. The value of GPCP precipitation data sets for climate studies is largely determined by how well it meets the project goals of consistency and completeness. Its major limitation for climate studies is its relatively short record length of only 17 years if one insists on consistent satellite and gauge input data. In this Chapter we provide a synthesis of GPCP-based climate studies and an assessment of the strengths and weaknesses of GPCP precipitation estimates for climate variability studies at various temporal and spatial scales. The technical details of constructing the GPCP data set and determination of instrument errors were discussed in Chapter 2.

Despite the care taken in constructing the GPCP data set, it has constraints associated with the real-world operations of the various satellite systems that feed into these data. These constraints arise from differences in satellite orbital characteristics, fields of view, spatial sampling, pixel size and temporal sampling. Consistency in the data set is also hampered by the changes in satellite sensors utilized during the span of the project and by changes in sensor characteristics as the instruments aged. The single largest potential source of instrument-related inconsistencies in the temporal record of precipitation estimates is associated with the lack of PMW data for precipitation estimates before July of 1987.

The land component of the precipitation estimates strongly depends on the gauge network of meteorological observations. The rain gauge measurements are certainly the most direct and thus might be thought of as the most reliable. However, the networks of stations, comprised mainly of first-order weather stations, have locations determined by aviation requirements and other operational constraints and are not ideally suited for optimal sampling of global precipitation over land. In addition, these measurements are very sensitive to instrumentation, site exposure and procedures (e.g., Sevruk 1989; Beck et al. 2005). Among the problems with the gauge networks is the decrease over time in the number of routine observations available from many regions of the world. In some regions weather services have instituted major changes in gauge networks without extensive inter-calibrations with older systems. For example, the movement away from the simple "bucket" gauges to more sophisticated instruments in several weather services potentially introduces undocumented biases in the historical gauge data network.

Despite these limitations, the GPCP data set is clearly one of great value to studies of climate variability on several temporal and spatial scales. Both the strengths and limitations of these data are discussed and summarized in the following sections.

3.2 Global Mean Precipitation and Its Distribution

3.2.1 The Global Mean Precipitation Rate

Since GPCP provides precipitation values over the globe, it is able to produce spatially complete estimates of mean global annual precipitation rate, a fundamental parameter for the study of global climate. The GPCP data provide a distinct advantage over estimates based solely on land-based gauges for the global mean daily precipitation rate, **P**. The estimate of **P** in the GPCP data is 2.61 mm day^{-1} (Adler et al. 2003). Interestingly, estimates for the more recent part of the record,

(1988 - 2003), which include PMW data absent from the first part of the record, result in the same the global average value, 2.61 mm day^{-1}, as the entire 1979 -2003 period. (See Table 3.1)

As discussed in Adler et al. (2003) there are significant differences between the land-only GPCP estimates, 2.09 mm day^{-1}, and traditional land-based gauge climatologies of Legates and Wilmott (1990) and Jäger (1976), who obtain 2.32 mm day^{-1} and 2.13 mm day^{-1} respectively. More recent gauge-based estimates by Beck et al. (2005) show an estimate of 2.12 mm day^{-1}, in closer agreement to the Jäger and GPCP land only estimates. Huffman et al. (1997) and Janowiak et al. (1995) suggest that the Legates and Wilmott based global land-only gauge estimates are biased by island-based rainfall estimates for the central Pacific. It should be noted that the operationally generated CMAP data (Xie and Arkin 1997) give lower land-only estimates of 1.95 mm day^{-1}, in part, because the CMAP values are not corrected for under catch. However, differences between the estimates are difficult to interpret given that CMAP tends to overestimate precipitation over land areas with few gauge observations such as western Africa (Yin et al. 2004).

TABLE 3.1. Mean rainfall (mm day^{-1}) over land and ocean (1988-2003)

	Globe	25°S-25°N	25°S-50°S	50°S-90°S	25°N-50°N	50°N-90°N
GPCP	2.61	3.12	2.6	2.07	2.33	1.75
CMAP	2.61	3.55	2.47	1.11	2.19	1.25
SSM/I	—	3.10	2.40	—	2.41	—
Mean	**2.61**	**3.25**	**2.49**	**1.59**	**2.31**	**1.50**

If we neglect the Legates and Wilmott (1990) values for the reasons given above, the land-only estimates range from 1.95 mm day^{-1} to 2.13 mm day^{-1}. The range of estimates, 0.18 mm day^{-1}, is roughly 9% of the mean, providing a conservative estimate of the uncertainty for mean precipitation over land. If we assume the same percentage uncertainty for **P** everywhere, then we arrive at the global mean daily rate of 2.61 ±- 0.23 mm day^{-1}. However, we believe the uncertainty to be much smaller if we explicitly include the satellite based estimates over water as discussed below.

If we include only estimates of **P** based on satellite data for the 1979 -2003 period, i.e. GPCP (2.61 mm day^{-1}) and CMAP (2.65 mm day^{-1}), then the range of estimates for **P** is reduced significantly to 0.04 mm day^{-1} or about 2% of the mean. **P** estimates based on SSM/I data (Ferraro 1997) are 2.49 mm day^{-1} widening the range of uncertainty to 0.16 mm day^{-1} or roughly 6% of the mean. We note that the GPCP and CMAP estimate include station data over land while the SSM/I do not. We also note that the SSM/I estimates have larger uncertainties at mid- and high- latitudes, particularly in the boreal winter.

It can be argued from global energy considerations that, to first approximation, **P** should have remained more or less constant over the 25-year observation period discussed here. In particular in an analysis of global energy budgets and current model simulations Allen and Ingram (2002) suggest that the range of observed and modeled changes in temperature is too small to even identify the relationships between greenhouse-related temperature and precipitation changes. They further caution that the range of uncertainty in estimates of equilibrium precipitation change associated with global change is extremely large, ranging from 0.6% to 18%. In fact, an examination of the GPCP 25-year global-mean record shows no statistically significant global trends of either sign and that the year-to-year variations in **P** are indeed small with a standard deviation for interannual variability of 0.03 mm day^{-1}. This estimate of interannual variability, 1% to 2% of the mean, is likely to be an overestimate of true interannual variability in **P** since it includes the uncertainties in the estimates GPCP.

3.2.2 The Global Distribution of Mean Precipitation

The GPCP data provide quantitative estimates of precipitation over the globe and were the first to provide spatially complete continuous estimates of the patterns of rainfall over the oceans. These data provide a baseline against which global climate models for climate change studies can be measured. That is these models need to demonstrate that they can replicate the correct distribution of monthly mean rainfall before they can be expected to provide useful information on how the climate may change.

In the deep tropics the total (land plus ocean) and ocean-only zonal mean annual precipitation reflects the mean position of the convergence zones with off-equatorial maxima and a relative minimum on the equator (Fig. 3.1a). In contrast, the land-only zonal mean profile shows a single maximum centered on the equator. Maxima appear in mid-latitudes of both hemispheres in both the ocean- and land-only zonal mean profiles reflecting the mean position of the storm tracks. A comparison of the zonal mean annual precipitation for the 1979 to 1986 period to the 1988-2003 period (Fig 3.1b) suggests that the SSM/I data has its greatest influence on the ocean estimates in the tropics and land estimates at mid- to high-latitudes during the latter period. The 1988-2003 estimates show slightly larger values of precipitation in the convergence zones and slightly lower values over the land areas. Over land the introduction of the GHCN-CAMS data prior to 1988 may have also influenced the magnitude differences.

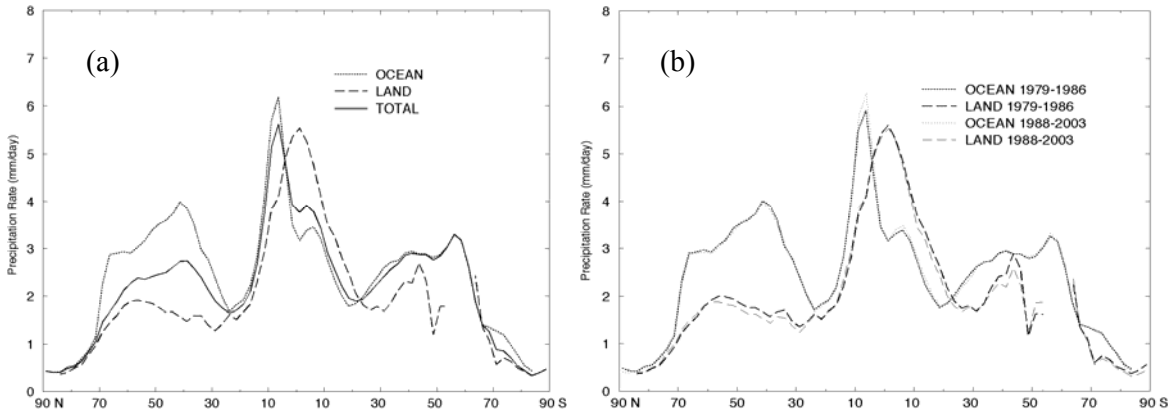

FIGURE 3.1. a) GPCP Zonal Mean Precipitation (mm day^{-1}) for the 1979 to 2003 period, total – solid line, land-only-dashed, ocean-only dotted, after Adler et al. (2003). b) Comparisons of Zonal Mean Precipitation for the 1979 to 1986 (heavy dotted-ocean, heavy dashed-land) periods versus 1988 to 2003 (light dotted-ocean, light dashed-land). Courtesy of Scott Curtis.

The annual mean distribution of GPCP precipitation (January 1979 through December 2003) indicates that the wettest parts of the planet are the western tropical Pacific, the eastern Pacific ITCZ area extending into the Amazon, and over the extreme eastern tropical Indian Ocean (Fig. 3.2). The data also reveal a relative minimum in West Pacific precipitation stretching from Jakarta northward to past the Celebes that breaks up the region previously depicted as one continuous precipitation maximum stretching from east of New Guinea to west of Sumatra. In the Northern Hemisphere, mid-latitude storm tracks associated with the Kuroshio and Gulf Stream currents are clearly visible along the eastern coastal regions of Asia and North America, respectively. In the Southern Hemisphere, the South Atlantic Convergence Zone and the South Pacific Convergence Zone are both apparent as local precipitation maxima that extend southeastward from southern Brazil and southeastward from New Guinea, respectively. Conversely, three couplets of very low precipitation straddle the equator in the extra-tropics that are centered in longitude near the Greenwich Meridian, 90^{o}E and 120^{o}W. These dry regions are

associated with the semi-permanent anticyclones that are located in those locations. Relatively dry conditions are also observed poleward of 60° latitude over both hemispheres.

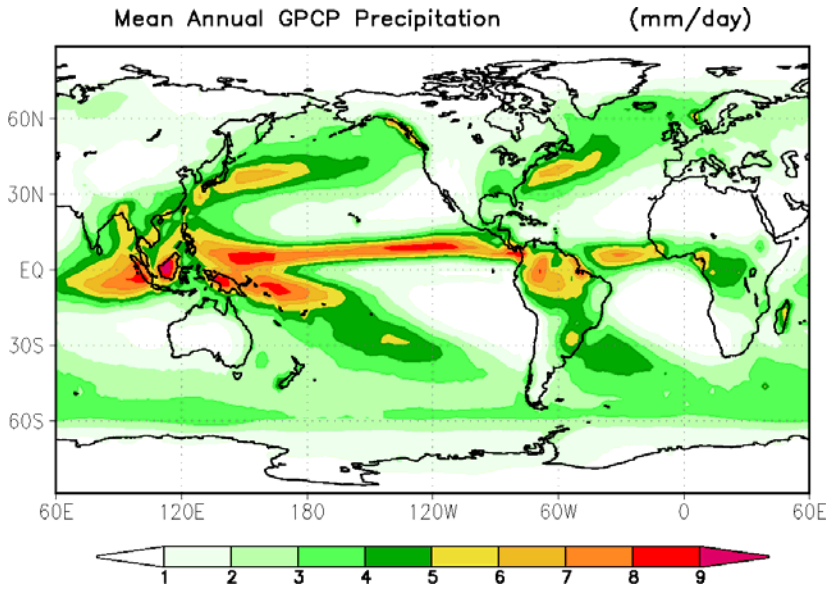

FIGURE 3.2. Mean annual GPCP precipitation over the period 1979-2003 in mm day^{-1}.

As mentioned above, the first eight years of the GPCP record does not contain PMW-based estimates of precipitation. We examine the mean spatial distribution of precipitation for three eight-year periods to compare the earlier part of the record to records of comparable length which include PMW data. There are great similarities in the overall spatial distribution of the precipitation for the three periods, 1979 – 1986, with no PMW estimates of precipitation, and the two 8-year periods, 1988 – 1995 and 1996 – 2003, that include PMW data (Fig 3.3). The first and last 8-year periods included the second-largest (1982-83) and largest (1997-98) El Niño/Southern Oscillation (ENSO) episodes of the 20th century respectively. To first approximation, the differences between the precipitation patterns of the first and second 8-year period (Fig 3.4a) reflect the strong 1982 – 83 ENSO in the former period with no counterpart in the later. With the exception of the regions influenced by ENSO there do not appear to be large systematic differences in these patterns that might be attributed to the lack of PMW data in the first 8–year period. In general, the largest differences occur in the tropics. Elsewhere the differences tend to be less than 0.5 mm day^{-1} with the west coast of the United States being a notable exception. However we note that given the overall lower precipitation rates at higher latitudes the smaller magnitudes of differences between the first period and later two are likely to have relatively larger impacts on zonal trend computations at these latitudes or differences expressed as percent of the mean.

In comparing the later two eight year periods (Fig 3.4b) again the bulk of the differences in the precipitation patterns are consistent with existence of a strong ENSO episode in one 8-year period, 1996 – 2003 in this instance. The larger magnitudes in the differences over the tropics in the latter periods compared to the differences between the first and second 8-year periods reflect the relative strength of the 1997/98 ENSO relative to the 1982/83 episode. High latitude differences in precipitation are generally larger in magnitude than in the comparisons between the first two 8-year periods. Since both of these later periods include the same satellite data inputs, these differences also reflect climate variability other than that directly associated with ENSO. Comparisons between the first and last 8-year periods reflect the larger magnitude of the 1997/98 ENSO versus the 1982/83 episode as well any biases associated with the lack of PMW data in the first period

(Fig 3.4c). However, part of the differences may also reflect a change from two TOVS satellites to one in March 1999.

3.3 Mean Annual Cycle

The mean annual cycle of globally averaged precipitation shows only small month-to-month variations about the 24-year period mean, **P,** of 2.61 mm day^{-1}. The uncertainties in the precipitation estimates, an estimate of which based on the discussion presented in sections 3.2.1 above, is given by the vertical arrow in Fig. 3.5a, are of comparable magnitude to variations seen in the mean annual cycle. Thus, the GPCP data do not reveal any significant mean annual cycle in the global precipitation. This leads to some interesting consequences with respect to the mean annual cycle by hemisphere (Fig. 3.5b). For example, both hemispheric means show strong annual cycles with equal mean amplitudes of about 1.3 mm day^{-1}. Since there is virtually no global mean annual cycle in these data the amplitudes of the hemispheric mean annual cycle of precipitation are virtually identical despite the vastly different distribution of land and water in each hemisphere. As a further consequence, the hemispheric mean annual cycles are exactly one-half cycle out of phase in the monthly mean GPCP data. In the Southern (Northern) Hemisphere the precipitation maximum (minimum) occurs in March while the Southern (Northern) Hemisphere minimum (maximum) occurs in August. We note that the hemispheric extremes are asymmetric with respect to the mean annual cycle i.e. in the Southern Hemisphere the minimum follows the maximum by 5 months (March to August) while in the Northern Hemisphere the minimum follows the maximum by 7 months (August to March). Precipitation is roughly equal in both hemispheres in early May and late November.

3.3.1 Total, land-only and ocean-only mean annual cycle of precipitation

The mean annual cycle of precipitation averaged over just land areas is dominated by the Northern Hemisphere (Fig. 3.5c). Peak precipitation occurs in July to August (near 2.3 mm day^{-1}) and minimum precipitation in December (slightly less than 2.0 mm day^{-1}). This is in good agreement with the mean annual cycle of an independent gauge-only analysis (Grieser and Beck 2006) revealing a minimum of 1.92 mm in November and exceeding 2.1 mm only from June to September. The mean annual cycle of ocean-only precipitation shows a much weaker amplitude (about 0.2 mm day^{-1}) with a minimum near 2.7 mm day^{-1} in July, a relative minimum in February and maxima near 2.9 mm day^{-1} in both March and November. We note that the July minimum in the ocean-only annual cycle coincides with the maximum in the land-only values. However, the ocean-only maxima straddle the December land-only minimum.

3.3.2 Annual Cycle of zonally averaged precipitation

The mean annual cycle of the zonal averaged precipitation (Fig. 3.6a) shows, as expected, that the mean precipitation rate is greatest in the near-equatorial tropical belt during all months of the year. In the Southern Hemisphere this precipitation maximum occurs during January through March. During April near-equatorial zonal means are about the same magnitude in both hemispheres reflecting a tendency for a "double" ITCZ during this time of year. The highest precipitation rates reside in the Northern Hemisphere the remainder of the year. The most intense precipitation occurs during May through early September. Conversely, the extremely dry regions are located poleward of 60^{o} latitude in both hemispheres. Dry regions in the tropics and sub-tropics are centered near 20^{o}N during January to April, and centered near 15^{o}S during June to September. Other precipitation estimates, e.g. CMAP, show the same general character of the mean annual cycle but with slightly larger values of precipitation rates in the equatorial regions. The differences between the zonally averaged precipitation for the full period and the first eight and a half years (Fig 3.6b) show relatively more near-equatorial precipitation for all months of the year, with the exception of

June, in the later estimates i.e., those containing the PMW data. The January through March differences show less precipitation from roughly 30 to 45° North and relatively more precipitation from 60 to 70° North. Differences in the Southern Hemisphere were smaller and less systematic. This suggests that some of the Northern Hemisphere differences may reflect changes over land in the gauge-based estimates.

3.3.3 Seasonal Evolution of Mean Precipitation Patterns

The seasonal maps of GPCP estimated precipitation (Fig. 3.7) show details that could only have been guessed at before the advent of satellite derived precipitation estimates. Most revealing is the mean annual cycle of precipitation patterns over the oceans. However, not to be ignored are the links between these oceanic features and the precipitation patterns over land. Among the features delineated in the mean seasonal fields are:

1) Large precipitation amounts associated with Northern Hemisphere mid-latitude storm tracks throughout the year but especially during boreal winter (December to February),
2) Clear evidence that a substantial portion of the Indian summer monsoon rainfall occurs over the Bay of Bengal,
3) The oceanic inter-tropical convergence-zone-related rainfall is concentrated in the Northern Hemisphere throughout the year,
4) Rainfall over the Amazon Basin during austral summer (December to February) is comparable to the rainfall rates experienced in the Maritime Continent during that season and greater than Maritime Continental rates during austral autumn (March to May),
5) Precipitation over central Africa is notably less than over other tropical continental regions despite the known maximum of lightning there (Christian et al. 2003),
6) The mean annual cycle of precipitation in the Eastern Pacific north of the equator experiences an annual range in mean precipitation rates comparable to those experienced in monsoon areas in the absence of land-sea temperature contrast, and
7) The mean rainfall patterns over the Maritime continent and Western Pacific show considerable spatial structure.

With regard to this last point, it is still uncertain how much of the detailed structure in the Western Pacific rainfall patterns is a result of island topography and how much reflects shortcomings in our abilities to adequately estimate precipitation in regions with complex configurations of topographic features and ocean boundaries. However, the relative minimum in West Pacific precipitation stretching from Jakarta northward to past the Celebes, except for boreal winter, is reflected in the available gauge data for Indonesia in all seasons consistent with the GPCP estimates.

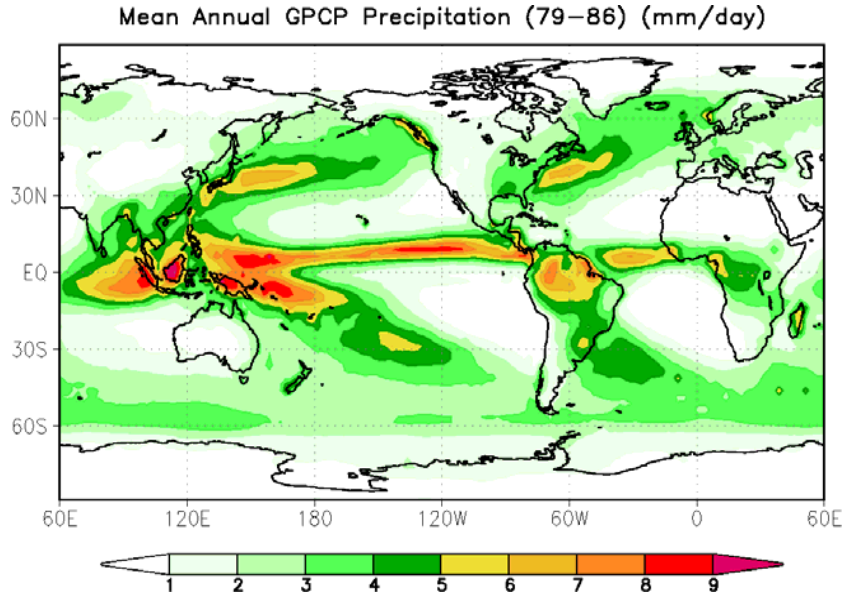

(a)

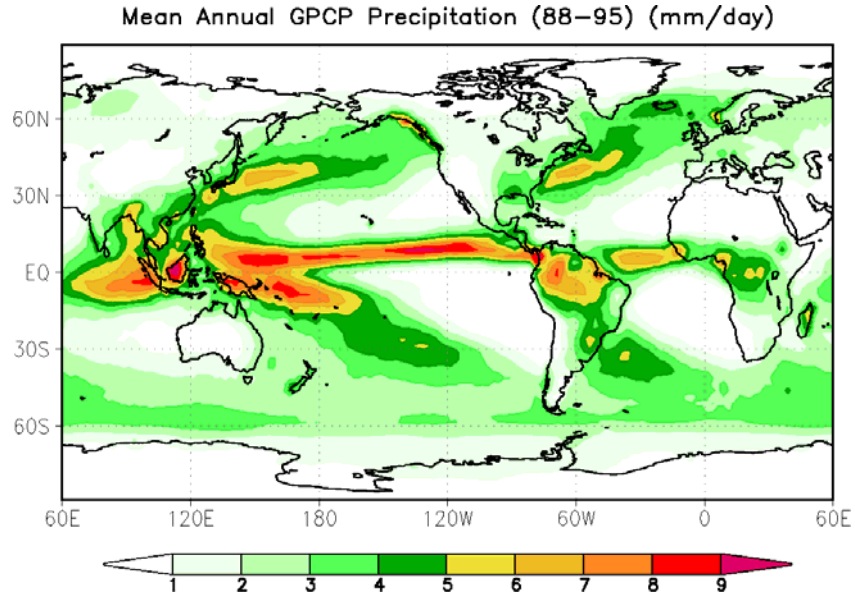

(b)

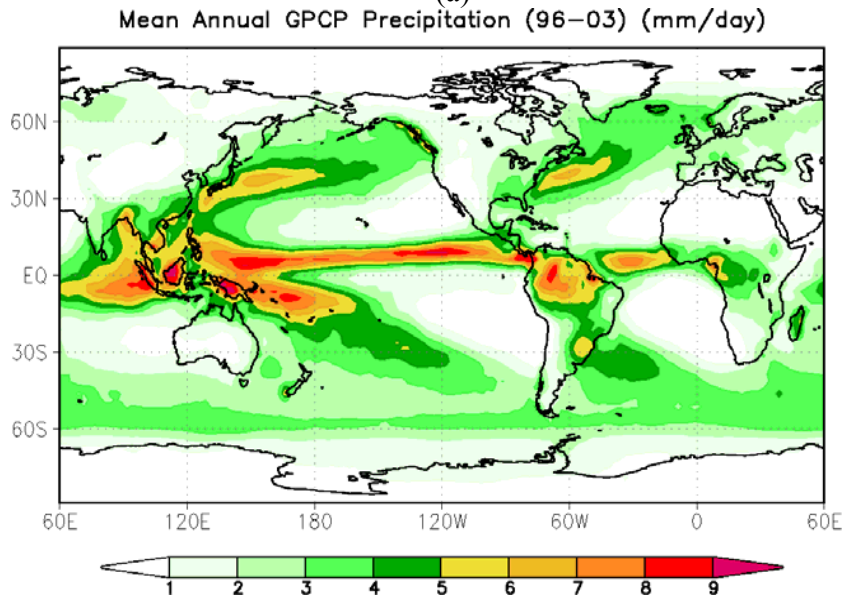

(c)

FIGURE 3.3. Global distribution of GPCP estimated precipitation for a) 1979 – 1986, b) 1987 – 1994, and c) 1995 – 2003.

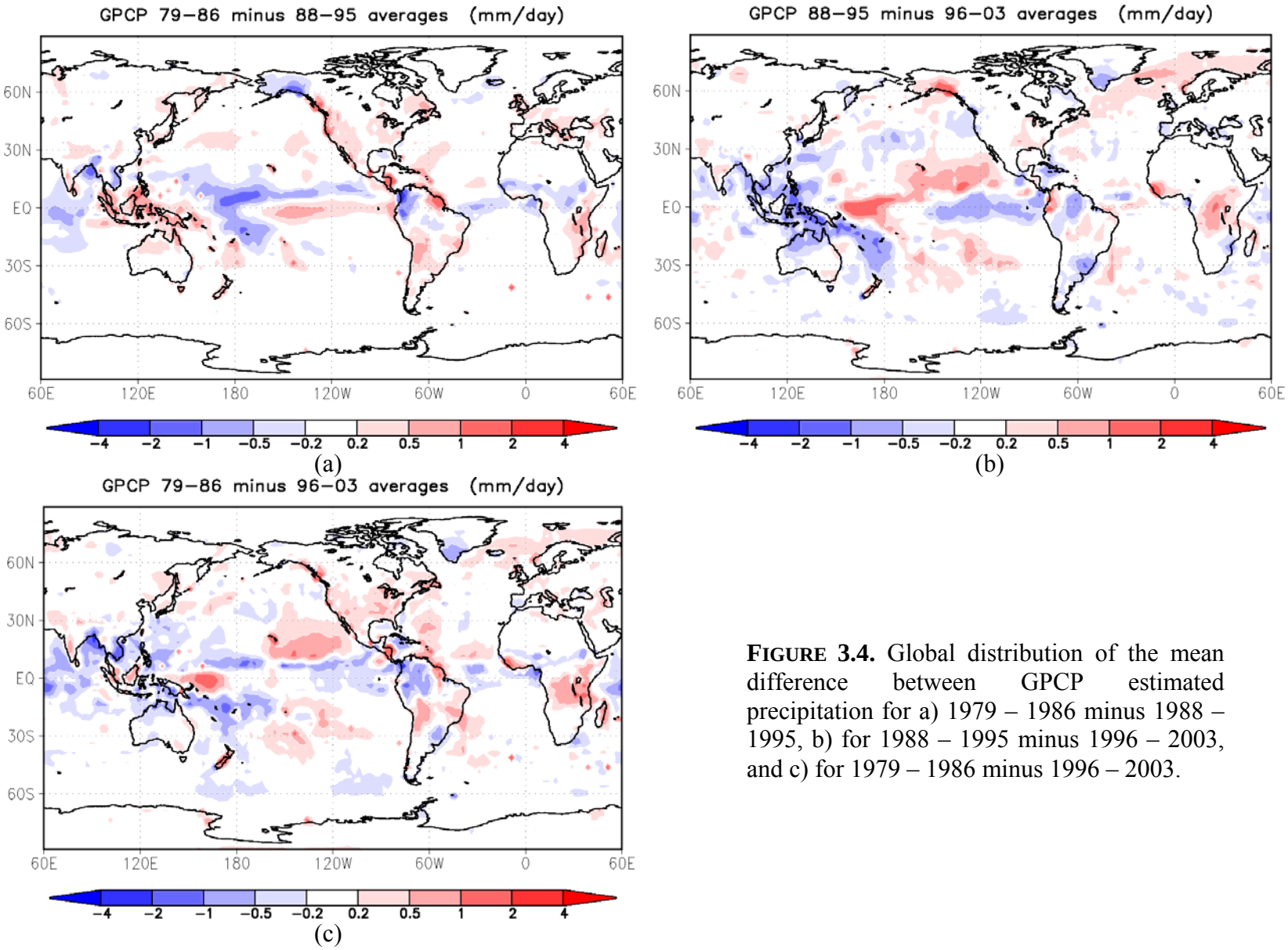

FIGURE 3.4. Global distribution of the mean difference between GPCP estimated precipitation for a) 1979 – 1986 minus 1988 – 1995, b) for 1988 – 1995 minus 1996 – 2003, and c) for 1979 – 1986 minus 1996 – 2003.

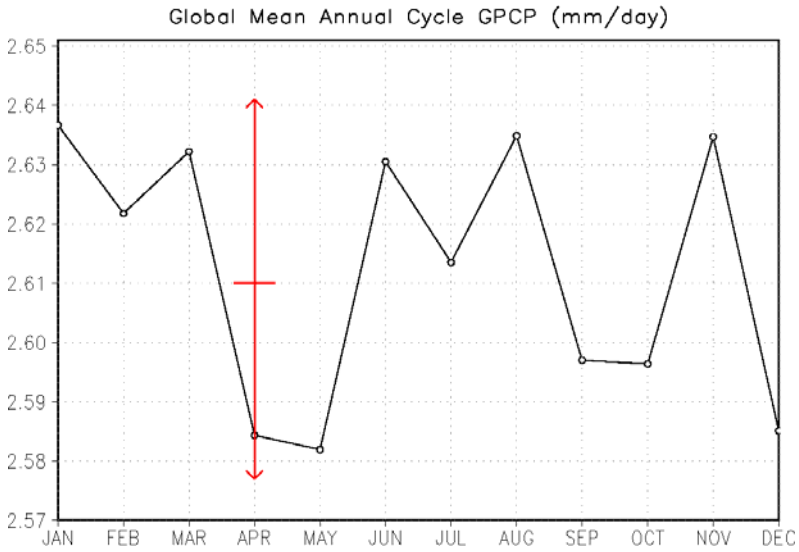

(a)

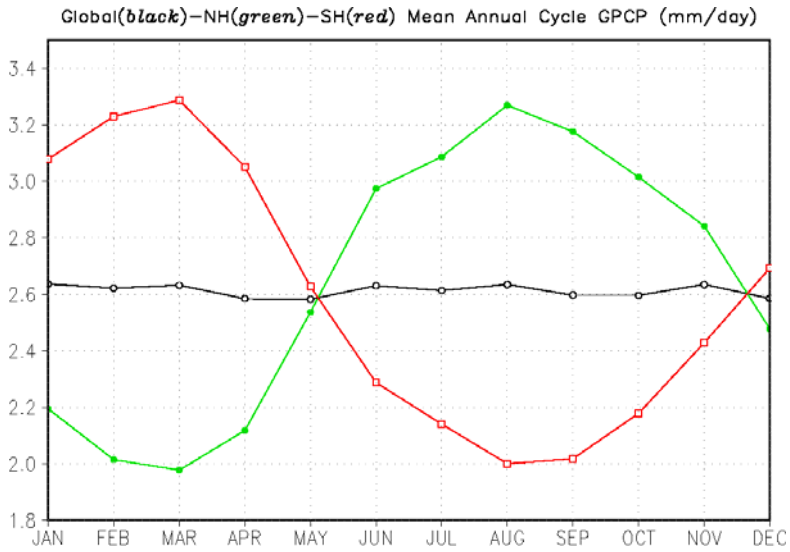

(b)

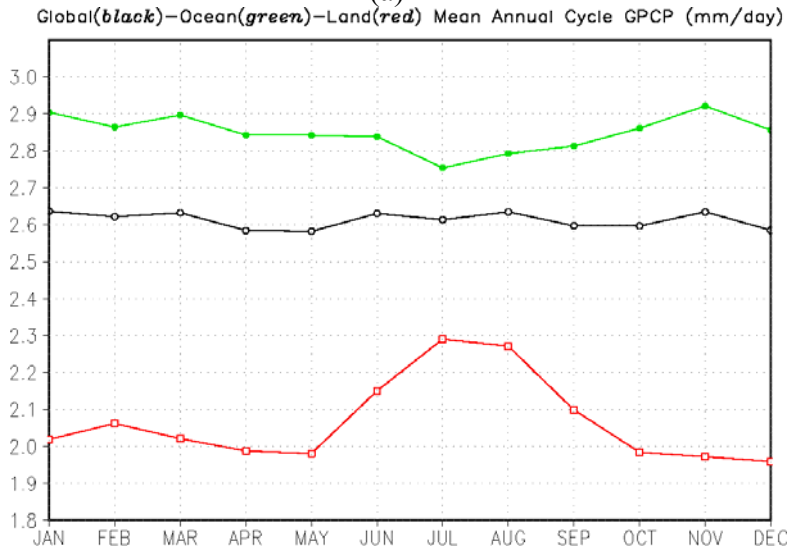

(c)

FIGURE 3.5. a) Mean annual cycle of GPCP precipitation on an expanded scale with an estimate of the uncertainty in these estimates represented by the vertical arrow; b) Mean annual cycle of GPCP precipitation i) global (black), ii) Northern Hemisphere (green), iii) Southern Hemisphere (red); c) Mean annual cycle of precipitation for Oceans (green), Global (black), Land (red).

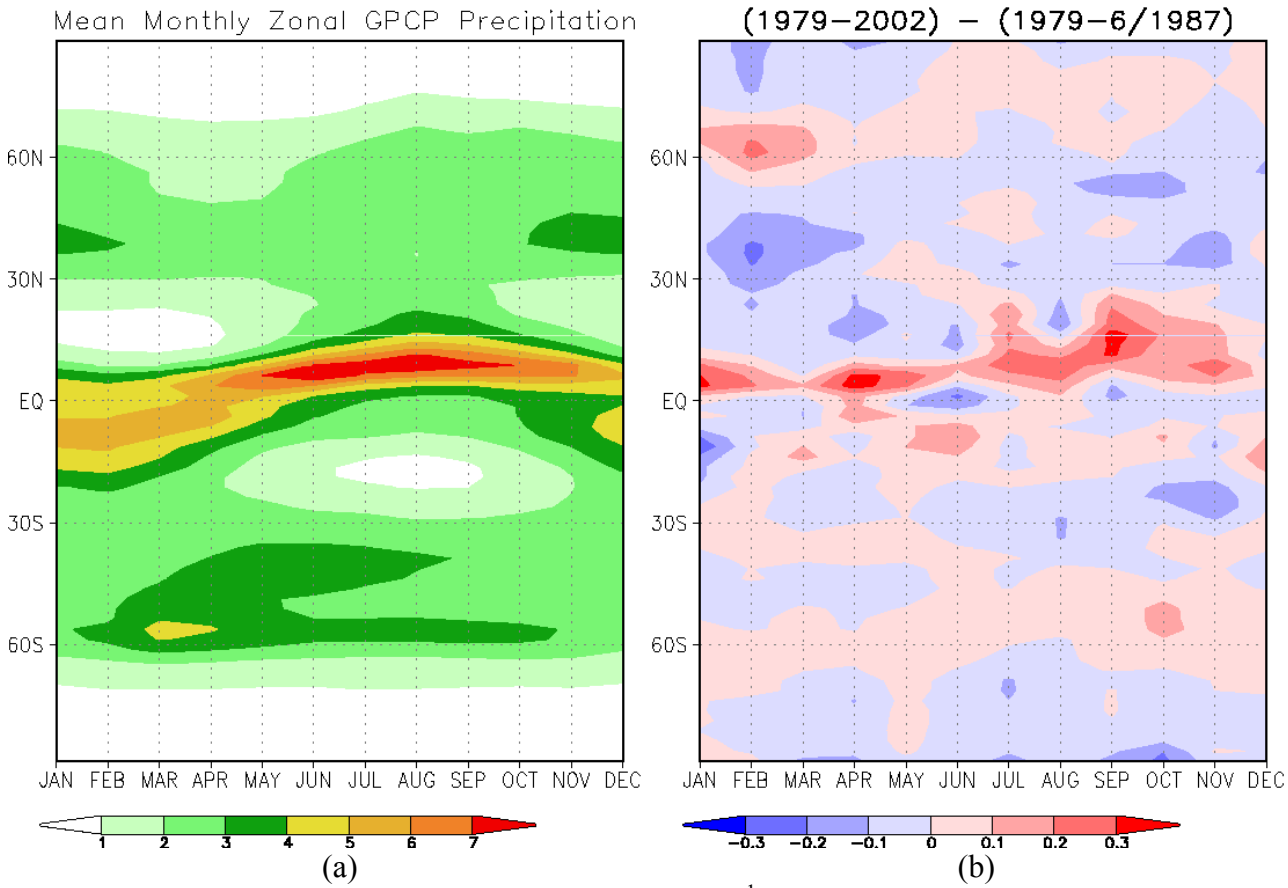

FIGURE 3.6. a) Annual cycle of zonally averaged precipitation (mm day^{-1}); b) Differences in the annual cycle of zonally averaged precipitation. The full period mean minus the early non-microwave data period (1979-1986/87).

3.4 Seasonal-to-Interannual Variability

As outlined in Section 3.2.1 above, the interannual variability of rainfall averages over the whole globe is very small in the GPCP 25 year record. However, constraints on the variability of the globally averaged mean precipitation rates do not limit the interannual variability in regional precipitation patterns. An estimate of the interannual standard deviation of precipitation (Fig. 3.8) based on the 25-year period 1979-2003 shows the greatest magnitude, greater than 5 mm day^{-1}, to be in the equatorial Pacific. This is no doubt related to interannual variability directly associated with ENSO. Secondary maxima in the standard deviation on the order of 1 to 2 mm day^{-1} are seen in regions generally teleconnected to ENSO including northeast and southeast South America, the Pacific Northwest and southern United States, southern Africa and parts of the greater Horn, much of Australia and India. Relative standard deviation maxima in the Congo, in locations along the west coast of Africa and in eastern Asia are likely due to ENSO teleconnections or other modes of climate variability undocumented before the availability of satellite-derived precipitation estimates.

3.4.1 Time series of global monthly anomalies

Ocean-only precipitation clearly dominates the GPCP time series over the globe and is clearly at a higher mean rate than over land (Fig 3.9a). The land-only series shows a vigorous annual cycle that is not easily discernable in either the ocean-only or total (global) time series. This is not surprising given the character of the mean annual cycles over land and ocean discussed in relation to Fig. 3.5b above. The land only and ocean only precipitation act in concert to produce a global-total time series that is smoother than either individually.

The time series of monthly mean tropical precipitation anomalies shows considerable month-to-month variability, generally within a range of ± 0.2 mm day^{-1} (Fig. 3.9b). Examination of the 12-month running mean global precipitation anomalies show some indications of low amplitude (less than 0.1 mm day^{-1}), low frequency (2-3 years) variability there is no apparent relationship between global precipitation anomalies and ENSO, e.g., the 12 month running mean values remain near zero in 1986/97 and 1997/98. The major volcanic eruptions of El Chichón and Mt Pinatubo, likewise, are not reflected in the global precipitation anomalies. On the other hand, land-only (ocean-only) observations show a clear tendency for dry (wet) conditions in association with ENSO.

3.4.2 Time series of zonal mean anomalies

There is no obvious indication of the change in satellite data inputs in June of 1987 in any of the global time series. However, an examination of the time series for zonally averaged land-only precipitation indicates clear discontinuities in the mean and variability associated with the introduction of the SSM/I data in the 25 – 50^{o} latitude bands in both hemispheres and poleward of 50^{o}N in the Northern Hemisphere (Fig 3.10). The change of character in the time series of the zonally averaged precipitation over land may also reflect some changes in the land station data. The time series zonally averaged GPCP for the ocean-only observations, also shown in Fig 3.10, do not indicate comparable obvious shifts in the mean level of rainfall. There are no obvious changes in the character of the time series of land-only and ocean-only precipitation poleward of 50^{o}S, (not shown) most likely reflecting the relatively small landmass in these latitudes.

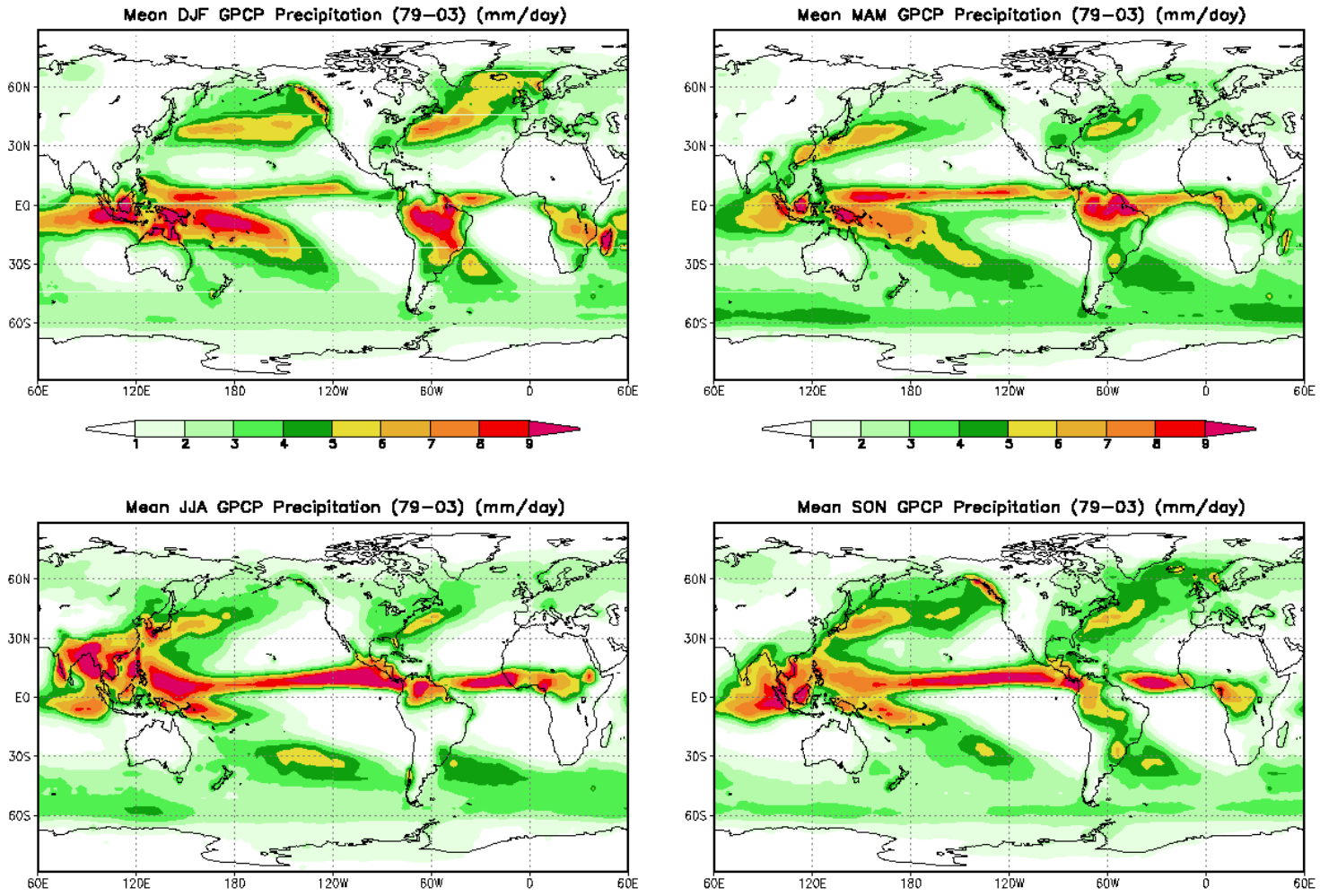

FIGURE 3.7. Seasonal mean precipitation (mm day^{-1}) for a) DJF, b) MAM, c) JJA, and d) SON.

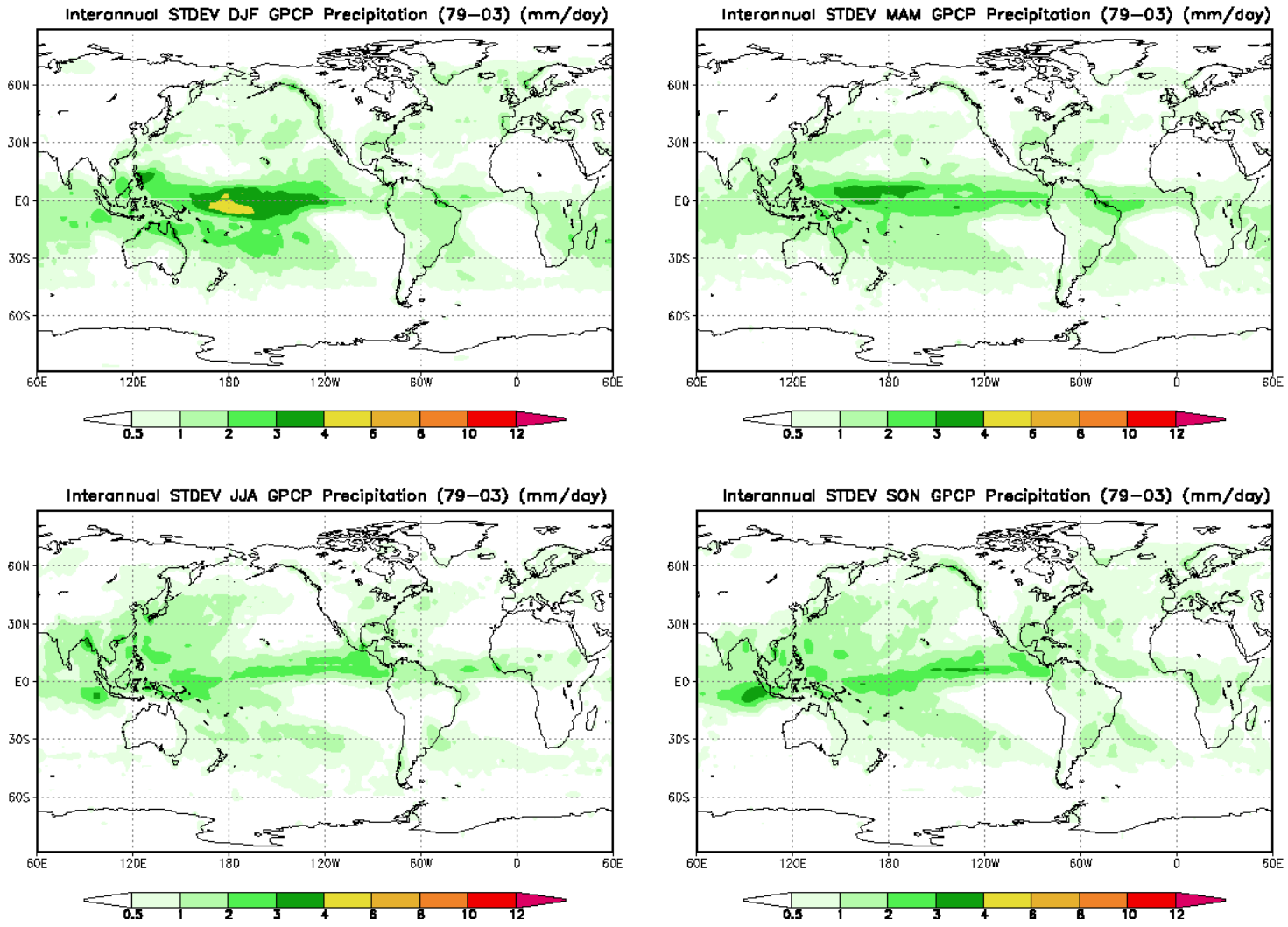

FIGURE 3.8. Standard deviations of GPCP precipitation estimates (mm day^{-1}) for a) DJF, b) MAM, c) JJA, and d) SON.

3.5 Low Frequency Variations and Trends

Prior to discussing low frequency and trends in the data it is worth emphasizing that while great care was taken in trying to produce the most complete and homogeneous record of precipitation the previous discussion in this chapter as well as Chapter 2 indicates that this data set was not specifically designed for trend monitoring. Nevertheless, in view of the importance of this topic it is appropriate to examine this data set for that possibility of low frequency variations and trends.

The time series of global annual mean GPCP precipitation shows no discernable trend (Fig 3.9a, and Adler et al. 2003). This doesn't preclude shifts in the large-scale precipitation patterns giving rise to regional tends. A map of global annual linear trends (Fig 3.11) is dominated by positive trends over the global oceans and negative over land areas. However, despite the obvious differences in pre- versus post- SSM/I in the land-only precipitation estimates discussed above only relatively small areas over land show trends significant at the 1% level. Small areas of statistically significant positive trend (1% level) appear over the Indian and central to eastern Pacific oceans. At least a portion of the trends in the eastern Pacific are likely associated with the larger magnitude of the 1997/98 ENSO compared to the 1982/83 episode. In addition we note that the pattern of linear trends has many similarities to the mean differences between the 1979 to 1986 and 1996 -2003 8-year means given in Fig 3.4c. Thus the "trend" may include the tendency for the later data, with SSM/I, to have higher precipitation estimates over tropical oceans and lower at mid-latitude land areas (Fig 3.1b) despite some efforts to calibrate these estimates against the SSM/I-based product from the later years.

As discussed above, the global linear trend over the 25-year data period is negligible. Linear trends computed for each grid-box show a relatively small number of grid-boxes that are statistically significant but it is likely that the analysis would not pass a field significance test (e.g., Livezey and Chen 1983). Gu et al. (2006) show statistically significant trends of 0.0373 mm day^{-1} $decade^{-1}$ for area averaged over 25^{o}N to 25^{o}S. Trends were computed after application of techniques to filter out the contributions of ENSO and volcanoes. However, interpretation of this analysis is also limited by issues of field significance discussed above and by the relatively short data set. It is well known that for short data sets linear trend analysis is very sensitive to the values at end points (e.g., Wunsch 1999; Percival and Rothrock 2005). Smith et al. (2006, and personal communication) examined the influence of changing the end points for linear correlation maps of GPCP data. They compute maps of linear trends based on the GPCP data for the entire period of record and compare them to the linear trend maps obtained by successively dropping one year at a time (Fig 3.12). They then compute the spatial correlations between the map derived from the entire series and those computed on the shorter periods. Their analysis shows a dramatic drop-off in the spatial correlations after 5 years of data have been "dropped" from the original analysis. By the time 9 years have been dropped i.e. comparisons of trends derived from the entire data set compared to the period with homogeneous satellite data (1988-2004) the spatial correlation drops to near 0.5, i.e. only 25% of the variance is in common between the two estimates of global trend patterns. This suggests that the GPCP record length is simply too short to provide stable estimates of trend based on linear trend patterns.

Nevertheless, in an EOF analysis of annual GPCP data for the 1979 to 2004 period Smith et al. (2006) find that roughly 51% of the total variance i.e., variability is represented by the first 3 EOFs, with the first two associated with ENSO. The third EOF accounts for 6% of the total variance and is associated with linear trends having a loading pattern very similar to that derived by simple linear trend analysis over the entire period discussed above, but in regions with weak variance they are greatly damped by the analysis. The trend in mode 3 was found to be significant at the 99% level

using the Mann – Kendall non parametric test (Mann 1945; Kendall 1975). They noted that the trend in the tropical western Pacific appeared to be related to increasing SST. Smith et al. do not test the sensitivity of the EOF analysis to the length of the record, analogous to the examination of the linear trends discussed above, but it is likely that this EOF pattern is also sensitive to the length of record. However, because of the damping of weak-variance regions and its ability to show variations from strict linearity, it should be less sensitive than linear-trend analysis. Nevertheless they urge caution about the interpretation of long period trends because of the length of record.

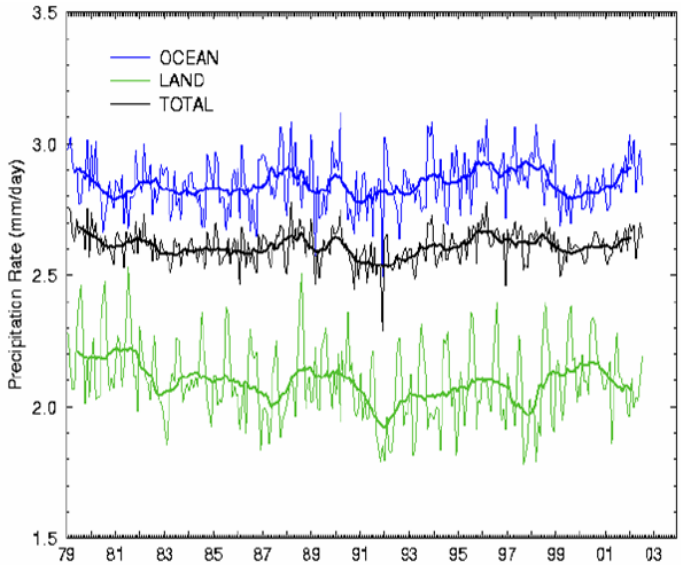

(a)

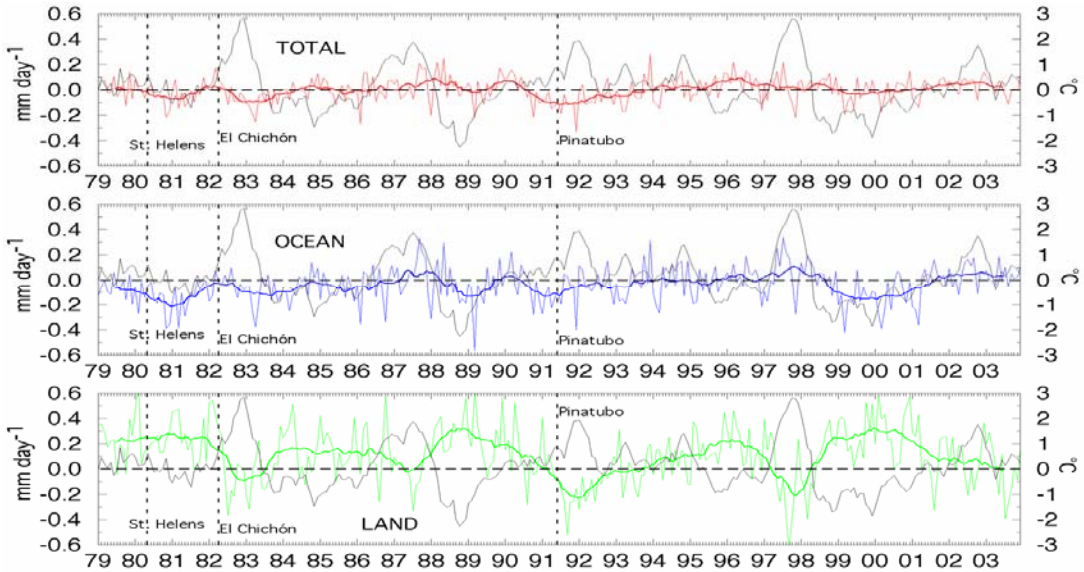

(b)

FIGURE 3.9. a) Global averages of monthly precipitation (mm day^{-1}) for ocean (blue), total (black), and land (green). Heavy lines indicate 12-month running mean. b) Tropical (30°N-30°S) averages of monthly precipitation anomalies (mm day^{-1}) for (top) total, (middle) ocean, and (bottom) land. Vertical dashed lines indicate the months of significant volcanic eruptions. The thin black curves indicate the Niño-3.4 SST index (°C). Heavy lines indicate 12 month running mean. (After Adler et al 2003).

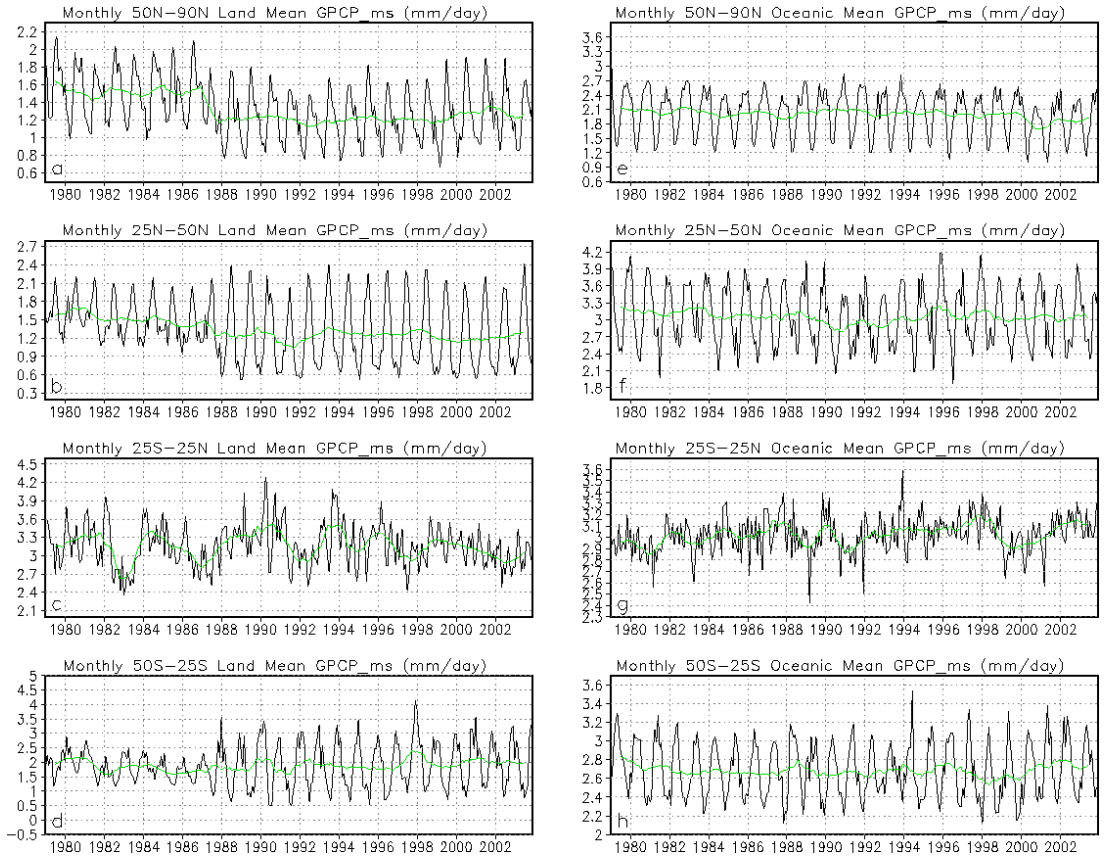

FIGURE 3.10. Time series of zonally averaged multi-satellite GPCP estimates over land (left hand panels) and over the ocean (right hand panels). Zonal averages are for 50° N to 90° N (a, e); 25° N to 50° N (b, f); 25° S to 25° N (c, g) and 25° S to 50° S (d, h). Given the small land mass areas at high southern latitudes (with the exception of Antarctica) zonal averages for 50° S to the pole are not given. Heavy lines are 12 month running mean.

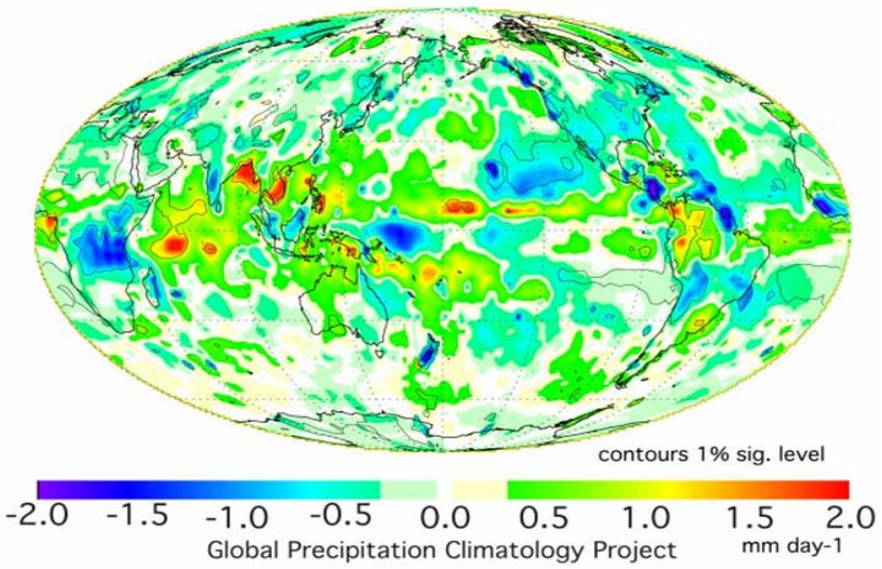

FIGURE 3.11. Map of linear trends in GPCP precipitation anomalies from January 1979 to December 2003. The thin black contour outlines the local 1% significance level. (Courtesy of Scott Curtis)

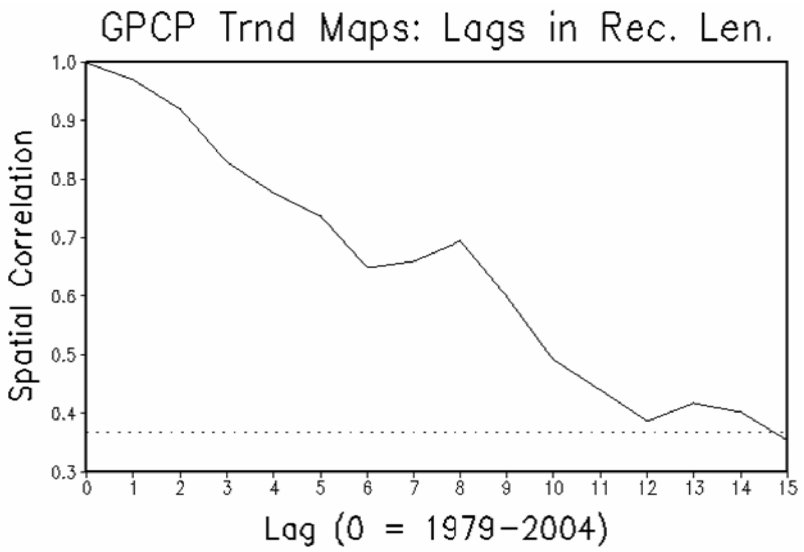

FIGURE 3.12. Spatial correlations between global trend maps computed for the 1979 to 2004 period and trends computed from successively fewer years. E.g., the spatial correlation at "lag" 1 is for the 1980 to 2004 period and so on. (Smith et al. 2006 and personal communication).

An analysis of the land-only trends based on the GPCC station data set (Beck et al. 2005) for the period 1979 to 1995 shows a number of areas of disagreement with the GPCP linear trend analysis for 1979 -2003 and the EOF analysis (Smith et al. 2006) discussed above. While there are some similarities to both GPCP analyses the difference in the linear trend patterns are consistent with the drop off in spatial pattern correlation one would expect given the 8-year difference in the GPCC and GPCP analyses presented above.

Considering global warming concerns the issues associated with low frequency variations and trends take on added importance. While there was some evidence of small regional trends, the brevity of the data record suggests that it is prudent not to declare that trends associated with global warming were observed in this data set, especially since the model studies mentioned above are not conclusive. On the other hand the fact that some low frequency variability over the oceans was observed with the suggestion that it may be related to increased sea surface temperature suggests that this data set, when extended, may have the potential to help determine the precise nature of the low frequency variability of precipitation, especially over the oceans. In fact an analysis of tropical rainfall characteristics using this data set by Lau et al. (2006) suggests that there was a positive trend in the upper 10% of rain rates and lower 5% of rain rates and a negative trend in the intermediate rain categories, with the total rain exhibiting essentially no change. This type of analysis will also benefit from a longer data record, which is crucial for accurate determination of trends, as pointed out by New et al. (2000) who studied long records of station data.

3.6 Summary and Concluding Remarks

The GPCP data have provided an opportunity to study the global precipitation patterns and their variability in ways that were not possible before the initiation of this data set. The care taken in providing the most consistent and complete precipitation analyses that the satellite and *in situ* data would allow have made this a "benchmark" data set for climate studies.

While suffering from some deficiencies, this data set is extremely useful for depicting the large scale distribution of precipitation and its interannual variation, especially over the oceans. Among the deficiencies that need attention is the accuracy estimates, especially over the oceans where only satellite based estimates are available. Incorporating results from the TRMM (Kummerow 1998) especially from the precipitation radar may help resolve some of the accuracy questions especially over oceans.

We conclude that the GPCP data is simply too short to provide a reliable estimate of global precipitation trends over land. Trend analyses of the oceans are difficult to interpret, with some of the trend patterns reminiscent of the rainfall shifts associated with the differences between the 1982/83 and 1997/98 ENSO. Nevertheless, there was some evidence cited that suggest that some useful low frequency information can be gleaned from the GPCP data. This is topic that requires further investigation and as the GPCP time series gets longer questions concerning longer period variability and trends can be answered with greater confidence.

Acknowledgements: This Chapter represents the synthesis of work by several contributors without whose help it would have been impossible to write this summary. Many thanks are due to G. Huffman, R. Adler, S. Curtis, X. Yin, J. Janowiak, P. Xie, R. R. Ferraro, P. Bauer, C. Beck, J. Grieser, B. Rudolf, M. Bell, M. B. Blumenthal, B. Lyon, F. R. Robertson, A. Gruber, and T. Smith.

Chapter 4. Future outlook

4.1 Introduction

Based on the preceding chapters it is clear that the GPCP global data set provides considerable new and useful information about the distribution and variability of global precipitation, particularly over the tropical oceans. These data, as described in Chapter 2, are a combination of various satellite estimates merged with gauges where available. This of course means that the ocean precipitation estimate is comprised of only satellite data.

The question that naturally comes to mind is what is the future outlook for this data set and global precipitation in general?

This chapter will attempt to address that question and hopefully provide a realistic glimpse into future possibilities for global precipitation estimation. It will first look at other available observations that might result in improvements of the current data set and then discuss new direct observations of precipitation from space that are anticipated from GPM in about 2013.

4.2 Improvements to the global data set

4.2.1 Observations

The global monthly mean data set assessed in this report is comprised of satellite estimates based on operational geostationary and polar orbiting spacecraft merged, over land, with rain gauge data.

The rain retrieval algorithms applied to the satellite data were developed as much as decades ago, based on the knowledge and data that then existed. However, as described in Chapter 2, there are many other retrieval algorithms utilizing a variety of techniques and data inputs. Some of these algorithms are designed for high spatial and temporal frequency and some for global application. Some are single channel algorithms (e.g., IR) and some are multi-spectral algorithms (e.g., combining IR, microwave and other spectral intervals).

There is also the TRMM data with its microwave imager, precipitation radar and IR sensors. It began providing rainfall estimates for the tropics in 1997. What is not known is whether these new data or algorithms can make improvements to the global precipitation data set. Finally, since the start of the GPCP project in 1986 the number of operational and research polar orbiting satellites carrying microwave and IR sensors has increased dramatically (see e.g., Table 2.1, Chapter 2, and Appendix III) providing improved temporal coverage not considered in the GPCP.

Similarly the in situ data used in the GPCP are based on gauges operated by national weather services and, while quality controlled by the GPCP for monthly mean estimates, their spatial coverage is variable. The GPCP also supports the collection of monthly mean gauge data from national collections to supplement the operational gauge data. While this increases the amount of gauge data by factors of 3 to 5 which improves gauge coverage, there are still large areas with significant gaps in coverage. There are also other gauge data sets, as described in Chapter 2, independent of the GPCP.

High quality 3-dimensional cloud and precipitation datasets from polarimetric radar are becoming more widely available. One use of these data is in the validation and subsequent improvement of satellite precipitation estimates, as has been done for TRMM (Wolff et al. 2005). Derived information on the physical properties of cloud droplets and hydrometeors will enable cloud

processes to be better represented in the models used to generate physical retrieval algorithms such as GPROF.

Improved observations of snow rate and precipitation in complex terrain are sorely needed. Current remote sensing and even gauge observations are deficient in this area. This is an area of research and development that the GPCP will be working on over the next several years.

The GPCP has devoted itself to producing an observational only data set so that it can provide a baseline for model comparisons. It requires analysis procedures to merge different sources of data that are generally discontinuous in space and time. Also, there is evidence that inclusion of precipitation output from numerical weather prediction models may actually improve rainfall estimates especially in middle and high latitudes. This was a topic of a recent workshop sponsored by GEWEX and the European Center for Medium Range Forecasting (Kanimitsu and Gruber 2003). Among the many important recommendations of that workshop a key one is:

> "Data assimilation methods holds the key to the future of precipitation analyses, since its greatest advantage is that it can provide the analysis of observed and derived meteorological variables (together with precipitation) in a dynamically, physically, and hydrologically consistent manner. However, it will take several more years before such analysis becomes as accurate as currently available observation only analyses. The GPCP will certainly accelerate this important development."

Clearly this is an area of future research that should receive considerable attention from the observational and modeling communities.

A reasonable assumption is that the GPCP can be improved with the inclusion of new observations and retrieval algorithms. The best way to demonstrate this is for the GPCP, which is a component of the Global Energy and Water Cycle Experiment Radiation Panel, to conduct a re-analysis of the monthly mean precipitation fields. As part of such a re-analysis new retrieval algorithms can be assessed for their accuracy and new gauge data sets can be incorporated and tested for their contribution to an improved global precipitation climatology. These results can also feed into to the pentad (Xie et al. 2003) and daily global (Huffman et al. 2001) estimates produced by GPCP (but not part of this assessment). Furthermore, given the increase of international operational polar orbiting and research satellites (see Appendix III) it may be possible to produce a global precipitation product with temporal resolution higher than daily e.g., three hourly. In fact researchers are involved in developing such data sets (e.g., http://precip.gsfc.nasa.gov, http://www.cpc.ncep.noaa.gov/products/global_precip/html/wpage.half_deg.html). This is an important and worthwhile endeavor and will require a significant international effort. In fact PEHRPP has already been initiated by the International Precipitation Working Group (IPWG) to evaluate current high resolution products. The detailed statistical evaluations will focus on regional sites but there are also plans to look at global high spatial and temporal resolution data by comparing monthly means of established data sets such as GPCP. The IPWG was organized as part of the Coordinating Group for Meteorological Satellites (CGMS) in 2001, and is concerned with development, validation and utilization of satellite based precipitation estimates.

4.3 Future Measurements from Space

4.3.1 Global Precipitation Mission

The most promising future measurements from space are those we can expect from GPM, (see for example Smith et al. 2007) and Fig 4.1. The following paragraphs are from the GPM web site, http://gpm.gsfc.nasa.gov/ where one can obtain more information about GPM. The GPM site

http://www.eorc.jaxa.jp/GPM/index_e.htm of the Japanese Aerospace Exploration Agency (JAXA) should also be consulted.

GPM will extend TRMM's observations of precipitation to higher latitudes, with more frequent sampling, and with focused research on providing a more complete understanding of the global hydrological cycle. GPM will be capable of measuring rain rates as small as a hundredth of an inch per hour to as large as 4 inches an hour. GPM will be able to estimate the various sizes of precipitation particles, and will also discriminate between snow and rain. GPM will seek to achieve these measurements with a 3-hour average revisit time over 80% of the globe, and the data will be available to users within 3 hours of observation time.

NASA and JAXA are working together to build and launch the GPM Core Satellite. The Core is the central precipitation-measuring observatory of GPM and will fly both a Dual-frequency Precipitation Radar (DPR) and a high-resolution, multi-channel PMW rain radiometer known as the GPM Microwave Imager (GMI). The Core will also serve as the calibration reference system for a constellation of support satellites. As was the case with TRMM, JAXA will provide the weather radar and possibly a launch vehicle while NASA will provide the PMW radiometer, the satellite superstructure, and the ground control segment.

In addition to the Core, a constellation of up to eight satellites will comprise the GPM sensor web. NASA plans to provide a dedicated member of the constellation. This is conceived as a relatively small spacecraft that will carry a single radiometer on board. The radiometer will be identical to the GMI on the Core. Other vehicles in the constellation are called *satellites of opportunity*, contributed by domestic agency partners such as NOAA and the U.S. Department of Defense, and GPM international partners. One specific example of a potential satellite of opportunity is the proposed French/Indian mission known as Megha-Tropiques. Each satellite of opportunity has its own unique scientific mission but will also contribute precipitation measurements to GPM. Each satellite in the constellation will carry one or more precipitation sensing instruments. At a minimum, to be a support satellite for the GPM constellation, a mission has to carry some type of PMW radiometer measuring several precipitation frequencies.

The GPM Mission will also frequently sample the "diurnal" or 24-hour variation in rainfall due to the rising and setting of the sun, by capitalizing on some satellite orbits that are synchronized with the sun, and others that are not.

4.3.2 The GPM Precipitation-Measuring Instruments

4.3.2.1 GPM Microwave Imager (GMI)

Microwave radiometers are versatile instruments, and when properly configured, can be used to infer a wide variety of phenomena in addition to precipitation, such as atmospheric moisture and temperature profiles, soil moisture, and sea surface temperature. To measure precipitation, the radiometer detects microwave energy emitted and scattered by rain and ice particles contained within clouds. This radiation continuously “upwells” from within clouds and is lost to space, but when intercepted and detected by a radiometer in Earth orbit, can provide useful information on the phase (liquid vs. solid), intensity and vertical distribution of precipitation. Several channels on board the radiometer measure microwave radiation at different wavelengths. Certain wavelengths are more sensitive to scattering or emission of microwave energy, and each wavelength is tuned to provide precipitation information within different vertical layers in the atmosphere.

Plans are in place to use microwave radiometers on several satellite missions that will be in orbit during the GPM era. NASA will procure two nearly identical GMI instruments from industry, one instrument to be placed on Core, and the other on the NASA constellation satellite. GMI will be designed to make simultaneous measurements in several microwave frequencies (e.g., 10.7, 19.3, 21, 37, 89 GHz), giving the instrument the capability to measure a variety of rainfall rates and related environmental parameters. Additional, there are plans to provide experimental, higher frequency channels (165 and 183 GHz) that have the needed sensitivity to detect light rain and snow frequently found at Earth's higher latitudes.

4.3.2.2 GPM Dual Frequency Radar (DFR)

Detailed measurements of cloud structure and precipitation characteristics will be made with DPR. JAXA is providing this instrument for GPM. The DPR is comprised of two, essentially independent radars operating in the microwave region of the electromagnetic spectrum. One radar transmits microwave energy in the Ku-Band (13.6 GHz) and is referred to as the Precipitation Radar (PR)-U. The other radar operates in the Ka-Band (35.55 GHz) and is referred to as the PR-A. Weather radar operates by measuring the amount of energy scattered back to the radar by precipitation. At the two different radar frequencies of the DFR, it is possible to infer information regarding rain rate, cloud type, solid vs. liquid precipitation, and the size of precipitation particles. The design of both radars builds upon the legacy of TRMM's Precipitation Radar (PR), but greatly extends its capabilities by incorporating new technologies and modifications for an expanded set of frequencies.

4.4 Concluding Remarks

A brief look at future possibilities for improved global precipitation has been presented. It has identified the most likely areas where one can expect significant improvement to our understanding of the distribution and variability of global precipitation within the next several years. It is, however, most likely not a complete identification of future possibilities of enhanced precipitation measurements. This may for example come from a microwave radiometer aboard geostationary satellites, or through an as yet unknown breakthrough in retrieval algorithms using hyperspectral data from instruments aboard NPOESS and GOES R. Moreover, special efforts are worth pursuing in the area of higher space-time resolution of the data set in cooperation with the IPWG PEHRPP (http://essic.umd.edu/~msapiano/PEHRPP/) providing the opportunity to link global and regional climate and weather issues. The influence of orography on the quality of satellite precipitation estimates is a scarcely tackled research theme, which needs far more attention in the future. Whatever the future holds the GPCP data set has set the foundation for global precipitation measurements, and one of the biggest challenges facing the scientific community is how to utilize new observations and science innovations to both improve and extend the existing global precipitation data.

References

Adler, R. F., and A. J. Negri, 1987: A satellite infrared technique to estimate tropical convective and stratiform rainfall. *J. Appl. Meteor.,* **27**, 30–51.

Adler, R. F., G. J. Huffman, and P. R. Keehn, 1994: Global tropical rain estimates from microwave-adjusted geosynchronous IR data. *Remote Sensing Rev.*, **11**, 125-152.

Adler, R. F., G. J. Huffman, A. Chang, R. Ferraro, P. Xie, J. Janowiak, B. Rudolf, U. Schneider, S. Curtis, D. Bolvin, A. Gruber, J. Susskind, and P. Arkin, 2003: The Version 2 Global Precipitation Climatology Project (GPCP) Monthly Precipitation Analysis (1979-Present). *J. Hydromet.*, **4**, 1147-1167.

Allen, M. R., and W. J. Ingram, 2002: Constraints on future changes in climate and the hydrologic cycle. *Nature*, **419**, 224-232.

Arkin, P. A., and B. N. Meisner, 1987: The relationship between large-scale convective rainfall and cold cloud over the western hemisphere during 1982-1984. *Mon. Wea. Rev*, **115**, 51-74.

Arkin, P. A., and P. Xie, 1994: The Global Precipitation Climatology Project: First Algorithm Intercomparison Project. *Bull. Amer. Meteor. Soc.*, **75**, 401–419.

Beck, C., J. Grieser, and B. Rudolf, 2005: A new monthly precipitation climatology for the global land areas for the period 1951 to 2000. DWD, *Klimastatusbericht KSB 2004*, 181 - 190.

Christian, H. J. R. J. Blakeslee, D. J. Boccippio, W. L. Boeck, D. E. Buechler, K. T. Driscoll, S. J. Goodman, J. M. Hall, W. J. Koshak, D. M. Mach, and M. F. Stewart, 2003: Global frequency and distribution of lightning as observed from space by the Optical Transient Detector. *J. Geophys. Res*., **108**(D1), 4005, doi:10.1029/2002JD002347

Cecil, D. J., E. J. Zipser, and S. W. Nesbitt, 2002: Reflectivity, ice scattering, and lightning characteristics of hurricane eye walls and rain bands. Part I: Quantitative description. *Mon. Wea. Rev.*, **130**, 769-784.

Chang, A. T. C., and L. S. Chiu, 1998: Non-systematic errors of monthly oceanic rainfall derived from SSM/I. *Mon. Wea. Rev*., **127**, 1630-1638.

Chang, A. T. C., L. S. Chiu, and T. T. Wilheit, 1993: Random errors of oceanic monthly rainfall derived from SSM/I using probability distribution functions. *Mon. Wea. Rev.,* **121**, 2351-2354.

Chiu, L. S., G. North, D. Short, and A. McConnell, 1990: Rain estimation from satellites: effect of finite field of view. *J. Geophys. Res.*, **95** (D3), 2177-2185.

Ebert, E. E., M. J. Manton, P. A. Arkin, R. J. Allam, G. E. Holpin, and A. Gruber, 1996: Results from the GPCP algorithm intercomparison programme, *Bull. Amer. Meteor. Soc*., **77**, 2875-2887.

Ferraro, R. R., 1997: SSM/I derived global rainfall estimates for climatological applications. *J. Geophys. Res*., **102**, 16,715-16,735.

Ferraro, R. R., and Q. Li, 2002: Detailed analysis of the error associated with the rainfall retrieved by the NOAA/NESDIS/SSMI algorithm: II. Rainfall over land. *J. Geophys. Res.,* **107**, 4680 – 4686.

Ferraro, R. R., and G. F. Marks, 1995: The development of SSM/I rain rate retrieval algorithms using ground based radar measurements. *J. Atmos. Oceanic Technol.,* **12**, 755-770.

Ferraro, R. R., N. C. Grody, and G. F. Marks, 1994: Effects of surface conditions on rain identification using the SSM/I. *Rem. Sensing. Rev.*, **11**, 195-209.

Ferraro, R. R., F. Weng, N. Grody, L. Zhao, H. Meng, C. Kongoli, P. Pellegrino, S. Qiu, and C. Dean, 2005: NOAA operational hydrological products derived from the AMSU. *IEEE Trans. Geosci. Remote. Sens.,* **43,** 1036 – 1049.

Griffith, C. G., W. L. Woodley, P. G. Grube, D. W. Martin, J. Stout, and D. N. Sikdar, 1978: Rain estimation from geosynchronous satellite imagery — Visible and infrared studies. *Mon. Wea. Rev.,* **106**, 1153–1171.

Grody, N. C., 1991: Classification of snow cover and precipitation using the Special Sensor Microwave/Imager (SSM/I). *J. Geophys. Res.,* **96,** 7423–7435.

Grieser, J, and C. Beck, 2006: Variability and triggering factors of observed global mean land-surface precipitation since 1951. DWD*, Klimastatusbericht KSB* 2005, 131-138.

Gruber, A., X. Su, M. Kanimitsu, and J. Schemm, 2000: The comparison of two merged rain gauge- satellite precipitation data sets. *Bull. Amer. Meteor. Soc*., **81**, 2231-2644.

Gu, G., R. Adler, G. Huffman, and S. Curtis, 2006: Tropical rainfall variability on interannual-to-interdecadal/longer-time scales derived from the GPCP monthly product. *J. Climate*, *20*, 4033-4066

Huffman, G. J., 1997: Estimates of root-mean-square random error for finite samples of estimated precipitation. *J. Appl. Meteor.*, **36**, 1191-1201

Huffman, G. J., R. F. Adler, B. Rudolf, U. Schneider, and P. R. Keehn, 1995: Global precipitation estimates based on a technique for combining satellite-based estimates, rain gauge analysis, and NWP model precipitation information. *J. Climate,* **8,** 1284–1295.

Huffman, G. J., R. F. Adler, P. A. Arkin, A. Chang, R. Ferraro, A. Gruber, J. E. Janowiak, A. McNab, B. Rudolf, and U. Schneider, 1997: The Global Precipitation Climatology Project (GPCP) combined precipitation dataset**.** *Bull. Amer. Meteor. Soc.,* **78**, 5–20.

Huffman, G. J., R. F. Adler, M. Morrissey, D. T. Bolvin, S. Curtis, R. Joyce, B McGavock, and J. Susskind, 2001: Global precipitation at one-degree daily resolution from multi-satellite observations. *J. Hydromet.,* **2**, 36-50.

Huffman, G. J., R. F. Adler, S. Curtis, D. T. Bolvin, and E. J. Nelkin, 2006: Global rainfall analyses at monthly and 3-hr time scales. Chapter 4 of *Measuring Precipitation from Space: EURAINSAT and the Future*, V. Levizzani, P. Bauer, and J. Turk, Ed., Springer Verlag (Kluwer Academic Pub. B.V.), Dordrecht, The Netherlands, accepted.

Iguchi, T., T. Kozu, R. Meneghini, J. Awaka, and K. Okamoto, 2000: Rain-profiling algorithm for the TRMM precipitation radar. *J. Appl. Meteor.*, **39**, 2038-2052.

Ikai, J., and K. Nakamura, 2003: Comparison of rain rates over the ocean derived from TRMM microwave imager and precipitation radar. *J. Atmos. Oceanic Technol.*, **20**, 1709-1726..

Jäger, L., 1976: *Monatskarten des Niederschlags für die ganze Erde*, Bericht des Deutschen Wetterdienstes, Vol 139, Offenbach a M., 33 pp plus Figures.

Janowiak, J. E., P. Arkin, P. Xie, M. Morrissey, and D. Legates, 1995: An examination of the east Pacific ITCZ rainfall distribution. *J. Climate,* **8**, 2810-2823.

Janowiak, J. E., A. Gruber, C. R. Kondragunta, R. E. Livezey, and G. J. Huffman, 1998: A Comparison of the NCEP–NCAR reanalysis precipitation and the GPCP rain gauge-satellite combined dataset with observational error considerations**.** *J. Climate*, **11**, 2960-2979.

Joyce, R. J., J. E. Janowiak, P. A. Arkin, and P. Xie, 2004: CMORPH: A method that produces global precipitation estimates from passive microwave and infrared data at high spatial and temporal resolution. *J. Hydromet.*, **5,** 487-503.

Kanimitsu, M., and A. Gruber, 2003: Report of the GEWEX-GPCP Workshop on Precipitation Analysis. March 11-13, 2003. WCRP Informal Report 11, 111 pages.

Kedem, B., L. Chiu, and G. North, 1990: Estimation of mean rain rate: application to satellite observations. *J. Geophys. Res.*, **95** (D2), 1965-1972.

Kendall, M. G., 1975: Rank correlation methods, *Charles Griffen Pub*., London, 202 pp.

Kidd, C., D. R. Kniveton, M. C. Todd, and T. J. Bellerby, 2003: Satellite rainfall estimation using combined passive microwave and infrared algorithms. *J. Hydromet.*, **4**, 1088–1104.

Kodama, Y.-M., and A. Tamaoki, 2002: A re-examination of precipitation activity in the subtropics and the mid-latitudes based on satellite-derived data. *J. Meteor. Soc. Japan,* **80**, 1261-1278.

Kongoli, C., P. Pellegrino, R. R. Ferraro, N. Grody, and H. Meng, 2003: A new snowfall detection algorithm over land using measurements from the Advanced Microwave Sounding Unit (AMSU). *Geophys. Res. Lett.*, **30,** 1756-1759.

Krajewski, W. F., G. J. Ciach, J. R. McCollum, and C. Bacotiu, 2000: Initial validation of the Global Precipitation Climatology Project monthly rainfall over the United States. *J. Appl. Meteor.*, **39**, 1071-1086.

Kummerow, C. D., W. S. Olson, and L. Giglio, 1996: A simplified scheme for obtaining precipitation and vertical hydrometeor profiles from passive microwave sensors. *IEEE Trans. Geosci. Remote Sens.,* **34,** 1213–1232.

Kummerow, C., W. Barnes, T.T.Kozu, J.Shiue,and J. Simpson, 1998: The Tropical Rainfall Measuring Mission (TRMM) sensor package. *J. Atmos. Ocean. Technology*, **15**, 809-817

Kummerow, C. D., Y. Hong, W. S. Olson, S. Yang, R. F. Adler, J. R. McCollum, R. R. Ferraro, G. Petty, D.-B. Shin, and T. T. Wilheit, 2001: The evolution of the Goddard Profiling Algorithm (GPROF) for rainfall estimation from passive microwave sensors. *J. Appl. Meteor.*, **40**, 1801-1820.

Kummerow, C. D., J. Simpson, O. Thiele, W. Barnes, A. T. C. Chang, E. Stocker, R. F. Adler, A. Hou, R. Kakar, F. Wentz, P. Ashcroft, T. Kozu, Y. Hong, K. Okamoto, T. Iguchi, H. Kuroiwa, E. Im, Z. Haddad, G. Huffman, B. Ferrier, W. S. Olson, E. J. Zipser, E. A. Smith, T. T. Wilheit, G. North, T. Krishnamurti, and K. Nakamura, 2000: The status of the Tropical Rainfall Measuring Mission (TRMM) after two years in orbit. *J. Appl. Meteor.*, **39**, 1965-1982.

Lau K.M. and H.T. Wu, (2006), detecting trends in tropical rainfall characteristics, 1979-2003. *Int. J. of Climatology*, DOI:10.1002/joc.1454.

Legates, D. R., 1987: *A Cimatology of Global Precipitation*. Publications in Climatology, **40**, University of Delaware, 85 pp.

Legates, D. R., and C. J. Willmott, 1990: Mean seasonal and spatial variability in gauge-corrected, global precipitation. *Int. J. Climatol.*, **10,** 111-127.

Li, Q., R. Ferraro, and N. C. Grody, 1998: Detailed analysis of the error associated with the rainfall retrieved by the NOAA/NESDIS SSM/I Rainfall Algorithm: Part I. Tropical oceanic rainfall. *J. Geophys. Res.,* **103**, 11,419-11,427.

Livezey, R. E., and W. Y. Chen, 1983: Statistical field significance and its determination by Monte Carlo techniques. *Mon. Wea. Rev.*, 111, 46–59.

Mann, H. B., 1945: Non parametric tests against trend. *Econometrica*, **13**, 245-259.

Masunaga, H., T. Iguchi, R. Oki, and M. Kachi, 2002: Comparison of rainfall products derived from TRMM microwave imager and precipitation radar. *J. Appl. Meteor*., **41**, 849-862.

McCollum, J. R., and R. R. Ferraro, 2003: The next generation of NOAA/NESDIS SSM/I, TMI and AMSR-E microwave land rainfall algorithms, *J. Geophys. Res.* **108,** 8382-8404.

McCollum, J. R., and R. R. Ferraro, 2005: Microwave rainfall estimation along coasts. *J. Atmos. Oceanic Technol.,* **22,** 497-512.

Mitchell, T. D., and P. D. Jones, 2005: An improved method of constructing a database of monthly climate observations and associated high-resolution grids. *Int. J. Climatol.*. **23**, 693-712.

Morrissey, M. L., M. A. Shafer, S. E. Postawko, and B. Gibson, 1995: The Pacific rain gage rainfall database. *Water Resources Res.*, **31**, 2111-2113.

Nesbitt, S. W., E. J. Zipser, and D. J. Cecil, 2000: A census of precipitation features in the tropics using TRMM: radar, ice scattering, and lightning observations. *J. Climate*, **13**, 4087-4106.

New, M., M. Hulme, and P. Jones, 2000. Representing twentieth-century space-time climate variability. Part II: Development of 1901-96 monthly grids of terrestrial surface climate. *J. Climate*, **13**, 2217-2238.

Nijssen, B., G. M. O'Donnell, D. P. Lettenmaier, D. Lohmann, and E. F. Wood, 2001: Predicting the discharge of global rivers. *J. Climate,* **14**, 3307–3323.

Olson, W. S., C. D. Kummerow, Y. Hong, and W.-K. Tao, 1999: Atmospheric latent heating distributions in the Tropics derived from satellite passive microwave radiometer measurements. *J. Appl. Meteor.*, **38**, 633–664.

Percival, D. B., and D. A. Rothrock, 2005: "Eyeballing" trends in climate time series: A cautionary note. *J. Climate*, **18**, 886-891.

Prabhakara, C., R. Iacovazzi, Jr., and J.-M. Yoo, 2002: TRMM precipitation radar and microwave imager observations of convective and stratiform rain over land and their theoretical implications. *J. Meteor. Soc. Japan*, **80**, 1183-1197.

Qiu, S., P. Pellegrino, and R. Ferraro, 2005: An evaluation of an improved AMSU rain rate algorithm and its application to winter season rainfall in the western United States. *Wea. Forecasting*, **20,** 761 – 774.

Reynolds, R. W., 1988: A real-time global sea surface temperature analysis. *J. Climate*, **1**, 75-86.

Rudolf, B., 1993: Management and analysis of precipitation data on a routine basis. *Proc. Int. WMO/IAHS/ETH Symp. on Precip. and Evap*., Slovak Hydromet. Inst., Bratislava, Sept. 1993, 1, 69-76.

Rudolf, B., H. Hauschild, W. Rüth, and U. Schneider, 1994: Terrestrial precipitation analysis: Operational method and required density of point measurements. In: Desbois, M. and F. Desalmand (Eds.): *Global precipitation and climate change. NATO ASI series I,* 26*,* Springer-Verlag, 173-186.

Rudolf, B., and U. Schneider, 2005: Calculation of gridded precipitation data for the global land-surface using in-situ gauge observations. *Proc. 2nd Workshop of the Int. Precipitation Working Group IPWG*, Monterey October 2004, EUMETSAT EUM P44, 231-247.

Rudolf, B., T. Fuchs, W. Rueth, and U. Schneider, 1998: Precipitation data for verification of NWP model re-analyses: The accuracy of observational results. *Proc. WCRP International Conference on Reanalyses*, Washington, DC, 27-31 Oct 1997, WMO/TD-No. 876, WCRP-104, 215-218.

Sauvageot, H., 1994: Rainfall measurement by radar: A review. *Atmos. Res.* **35**, 27-54.

Savage, R. C., and J. A. Weinman, 1975: Preliminary calculations of the upwelling radiance from rain clouds at 37.0 and 19.35 GHz. *Bull. Amer. Meteor. Soc.,* **56,** 1272–1274.

Scofield, R. A., 1987: The NESDIS operational convective precipitation estimation technique. *Mon. Wea. Rev*. **115**, 1773-1792.

Sevruk, B., 1989: Reliability of precipitation measurements. *Proc. WMO/IAHS/ETH Workshop on Precipitation Measurements*, St. Moritz (B. Sevruk, Ed.), 13-19.

Smith, E. A., G. Asrar, Y. Furuhama, A. Ginati, C. Kummerow, V. Levizzani, A. Mugnai, K. Nakamura, R. Adler, V. Casse, M. Cleave, M. Debois, J. Durning, J. Entin, P. Houser, T. Iguchi, R. Kakar, J. Kaye, M. Kojima, D. Lettenmaier, M. Luther, A. Mehta, P. Morel, T. Nakazawa, S. Neeck, K. Okamoto, R. Oki, G. Raju, M. Shepherd, E. Stocker, J. Testud, and E. Wood, 2007: International Global Precipitation Measurement (GPM) program and mission: An overview. In: *Measuring precipitation from space - EURAINSAT and the future.* V. Levizzani, P. Bauer, and F. J. Turk, Eds., Springer, 611-653.

Smith,T., X. Yin, and A. Gruber, 2005: Personal Communication.

Smith, T, X. Yin, and A. Gruber, 2006: Variations in annual global precipitation (1979-2004), based on the Global Precipitation Climatology Project 2.5^0 analysis. *Geophy. Res Lett*, **33**, L06705, doi:10.1029/2005GL025393.

Sorooshian, S., K.-L. Hsu, X. Gao, H. V. Gupta, B. Imam, and D. Braithwaite, 2000: Evaluation of PERSIANN system satellite-based estimates of tropical rainfall. *Bull. Amer. Meteor. Soc.*, **81**, 2035-2046.

Spencer, R. W., 1993: Global oceanic precipitation from the MSU during 1979-91 and comparisons to other climatologies. *J. Climate*, **6**, 1301-1326.

Toracinta, E. R., D. J. Cecil, E. J. Zipser, and S. W. Nesbitt, 2002: Radar, passive microwave, and lightning characteristics of precipitating systems in the tropics. *Mon. Wea. Rev.*, **130**, 802-824.

Turk, F. J., G. Rohaly, J. D. Hawkins, E. A. Smith, A. Grose, F. S. Marzano, A. Mugnai, and V. Levizzani, 2000: Analysis and assimilation of rainfall from blended SSM/I, TRMM and geostationary satellite data. *Proc. 10th Conf. Satellite Meteorology and Oceanography*, AMS, Long Beach, CA., 66-69.

Vicente, G. A., J. C. Davenport, and R. A. Scofield, 2001: The role of orographic and parallax correction on real time high resolution satellite rain rate distribution. *Int. J. Remote Sensing,* **23**, 221-230.

Vicente, G. A., R. A. Scofield, and W. P. Menzel, 1998: The operational GOES infrared rainfall estimation technique. *Bull. Amer. Meteor. Soc.*, **79**, 1883-1898.

Viltard, N., C. Kummerow, W. S. Olson, and Y. Hong, 2000: Combined use of the radar and radiometer of TRMM to estimate the influence of drop size distribution on rain retrievals. *J. Appl. Meteor*., **39**, 2103-2114.

Wang, S. A., 1995: Modeling the beamfilling correction for microwave retrieval of oceanic rainfall, Ph. D. Dissertation, Dept of Meteorology, Texas A&M University, College Station, TX, 99 pp.

WCRP, 1986: Report of the Workshop on Global Large Scale Precipitation Data Sets for the World Climate Research Program. WCP-11, WMO/TD-No.94, WMO, Geneva, 50pp.

Weinman, J. A., and P. J. Guetter, 1977: Determination of rainfall distributions from microwave radiation measured by the Nimbus 6 ESMR. *J. Appl. Meteor*., **16**, 437–442.

Wilheit, T. T., A. T. C. Chang, and L. S. Chiu, 1991: Retrieval of monthly rainfall indices from microwave radiometric measurements using probability distribution functions. *J. Atmos. Oceanic Technol.,* **8**, 118 – 136.

Wilmott, C. J., C. M. Rowe, and W. D. Philpot, 1985: Small-scale climate maps: A sensitivity analysis of some common assumptions associated with grid-point interpolation and contouring. *Amer. Cartographer*, **12**, 5-16.

Wolff, D. B., D. A. Marks, E. Amitai, D. S. Silberstein, B. L. Fisher, A. Tokay, J. Wang, and J. L. Pippitt, 2005: Ground validation for the Tropical Rainfall Measuring Mission (TRMM)**.** *J. Atmos. Oceanic Technol.,* **22**, 365–380.

Wunsch, C., 1999: The interpretations of short climate records with comments on the North Atlantic and Southern Oscillation. *Bull. Amer. Meteor. Soc.*, **80**, 245-255.

Xie, P., and P. A. Arkin, 1997: Global precipitation: a 17-year monthly analysis based on gauge observations, satellite estimates, and numerical model outputs. *Bull. Amer. Meteor. Soc*., **78**, 2539-2558.

Xie, P., and P. A. Arkin, 1998: Global Monthly Precipitation Estimates from Satellite-Observed Outgoing Longwave Radiation. *J. Climate*, **11**, 137–164.

Xie, P, J. E. Janowiak, P. A. Arkin, R. Adler, A. Gruber, R. Ferraro, G. J. Huffman, and S. Curtis, 2003: GPCP pentad precipitation analyses: An experimental dataset based on gauge observations and satellite estimates. *J. Climate*, **16**, 2167-2214.

Yin, X., A. Gruber, and P. A. Arkin, 2004: Comparison of the GPCP and CMAP merged gauge-satellite monthly precipitation products for the period 1979-2001. *J. Hydromet.*, **5**, 1207-1222.

Appendix I. Acronyms

AGPI	Adjusted GOES Precipitation Index
AMSR-E	EOS Advanced Scanning Microwave Radiometer
AMSU-A(B)	Advanced Microwave Sounding Unit A(B)
AVHRR	Advanced Very High Resolution Radiometer
CAMS	Climate Analysis and Monitoring System
CGMS	Coordination Group for Meteorological Satellites
CPTEC	Weather Forecast and Climate Studies Centre (of INPE, Brazil)
CMAP	CPC Merged Analysis of Precipitation
CMORPH	CPC Morphing technique
CPC	NWS Climate Prediction Center
CRU	Climate Research Unit
CST	Convective Stratiform Technique
DFR	Dual Frequency Radar
DPR	Dual Frequency Precipitation Radar
DMSP	Defense Meteorological Satellite Program
DOC	Department of Commerce, USA
DOD	Department of Defense, USA
DWD	Deutscher Wetterdienst
ECMWF	European Centre for Medium-Range Weather Forecasts
EDR	Environmental Data Record
ENSO	Enl Niño - Southern Oscillation
EOF	Empirical Orthogonal Function
EOS	NASA Earth Observing System
EPS	EUMETSAT Polar System
EUMETSAT	European Organization for the Exploitation of Meteorological Satellites
FAO	Food and Agriculture Organization of the UN
FNMOC	Fleet Numerical Meteorology and Oceanography Center
GEO	Geostationary Earth Orbit (also, a satellite in GEO)
GEWEX	Global Energy and Water Cycle Experiment
GHCN	Global Historical Climate Network
GHz	Giga Hertz
GMI	GPM Microwave Imager
GOES	Geostationary Operational Environmental Satellite
GPCC	Global Precipitation Climatology Centre
GPCP	Global precipitation Climatology Project
GPI	GOES Precipitation Index
GPM	Global Precipitation Mission
GPROF	Goddard Profiling Algorithm
GRP	GEWEX Radiation Panel
GSFC	Goddard Space Flight Center
GTS	Global Telecommunications System
HIRS	High resolution Infrared Sounder
IFFA	Interactive Flash Flood Analyzer
IJPS	Initial Joint Polar-Orbiting Operational Satellite System
INPE	Brazilian Institute for Space Research
IPCC	Intergovernmental Panel on Climate Change
IPO	tri-agency Integrated Program Office of DoC, DoD, and NASA
IPWG	International Precipitation Working Group

IR	Infrared
ITCZ	Inter-Tropical Convergence Zone
IWP	Ice Water Path
JAXA	Japanese Aerospace Exploration Agency
JMA	Japan Meteorological Agency
KLM	see NOAA KLM
LEO	Low Earth Orbit (also, a satellite in LEO)
LIS	Lightning Imaging Sensor
METEOSAT	EUMETSAT geostationary platform
MM5	NCAR/PSU Mesoscale Model Version 5
MODIS	EOS MODerate resolution Imaging Spectroradiometer
MS	Multi-Satellite
MTSAT	Multi-functional Transport Satellite
MVIRI	Meteosat Visible and InfraRed Imager
NASA	National Aeronautics and Space Administration, USA
NCAR	National Center for Atmospheric Research, USA
NCDC	National Climatic Data Center, USA
NCEP	National Centers for Environmental Prediction, USA
NESDIS	National Environmental Satellite Data and Information Service, USA
NOAA	National Oceanic and Atmospheric Administration (agency and satellite), USA
NOAA KLM	NOAA-15 (K), -16(L) and -17 (M) satellites
NPOESS	National Polar-orbiting Environmental Satellite System, USA
NWS	National Weather Service, USA
OLR	Outgoing Longwave Radiation
OPI	Outgoing Longwave Radiation (OLR) Precipitation Index
ORA	NOAA Office of Research and Applications
PEHRPP	Pilot Evaluation of High Resolution Precipitation Products
PERSIANN	Precipitation Estimation from Remotely Sensed Information using Artificial Neural Networks
PMW	Passive Microwave
PSPDC	Polar Satellite Precipitation Data Center
PSU	Pennsylvania State University
PR	TRMM Precipitation Radar
SEVIRI	Spinning Enhanced Visible and InfraRed Imager
SG	Satellite Gauge
SSM/I	Special Sensor Microwave/Imager
SSM/IS	Special Sensor Microwave/Imager Sounder
SSU	Stratospheric Sounding Unit
Tb	Brightness temperature
TIROS	Television Infrared Observation Satellite
TMI	TRMM Microwave Imager
TOVS	Television-Infrared Observation Satellite (TIROS) Operational Vertical Sounder
TRMM	Tropical Rainfall Measuring Mission
UN	United Nations
VAR	Variable Rain rate precipitation algorithm
VIRS	TRMM Visible and InfraRed Scanner
VIS	Visible
VISSR	Visible and Infrared Spin Scan Radiometer
WCRP	World Climate Research Programme
WMO	World Meteorological Organization

Appendix II. Contributors

Assessment Leads, Authors of Executive Summary and Chapter 1 (Introduction): Arnold Gruber (Cooperative Institute for Climate Studies, Earth System Science Interdisciplinary Center, University of Maryland, USA) and Vincenzo Levizzani (Institute of Atmospheric Sciences and Climate, Italian National Research Council, Bologna, Italy)

Chapter 2. Global Precipitation Data Sets
Lead Authors: Chris Kidd (School of Geography, Earth and Environmental Sciences, University of Birmingham, UK) and Kenji Nakamura (Hydrospheric Atmospheric Research Center, Nagoya University, Japan).

Chapter 2 Contributors:
Carlos Angelis (Centro de Previsão de Tempo e Estudos Climáticos, CPTEC, Brazil).
Phillip Arkin (Earth System Science Interdisciplinary Center, University of Maryland, USA)
Elizabeth E. Ebert (Bureau of Meteorology Research Centre, Melbourne, Australia)
Ralph Ferraro (NOAA/NESDIS, USA)
Jürgen Grieser (GPCC, Offenbach, Germany, now at FAO)
Arnold Gruber (Cooperative Institute for Climate Studies, Earth System Science Interdisciplinary Center, University of Maryland, USA)
George J. Huffman, (SSAI/NASA/GSFC, Greenbelt, USA)
John Janowiak (NOAA/NWS/NCEP/Climate Prediction Center, USA)
Paul Joe (Environment Canada)
Bruno Rudolf (GPCC, Offenbach, Germany)
Jorge Sánchez-Sesma (Instituto Mexicano de Tecnología del Agua, Morelos, México)

Chapter 3. Spatial and Temporal Variability of Precipitation
Lead Authors: C. Ropelewski (International Research Institute for Climate and Society, The Earth Institute of Columbia University, USA) and P. Arkin (Earth System Science Interdisciplinary Center, University of Maryland, USA)

Chapter 3 Contributors:
Robert Adler (NASA/GSFC, Greenbelt, USA)
Peter Bauer (ECMWF, Reading, UK)
Christoph Beck (GPCC, Offenbach, Germany)
Michael Bell (International Research Institute for Climate and Society, The Earth Institute of Columbia University, USA)
M. Benno Blumenthal (International Research Institute for Climate and Society, The Earth Institute of Columbia University, USA)
Scott Curtis (Department of Geography, East Carolina University, USA)
Ralph Ferraro (NOAA/NESDIS, USA)
Jürgen Grieser (GPCC, Offenbach, Germany)
Arnold Gruber (Cooperative Institute for Climate Studies, Earth System Science Interdisciplinary Center, University of Maryland, USA)
George Huffman (SSAI/NASA/GSFC, Greenbelt, USA)
John Janowiak (NOAA/NWS/NCEP/Climate Prediction Center, USA)
Brad Lyon (International Research Institute for Climate and Society, The Earth Institute of Columbia University, USA)
Franklin R. Robertson, (National Aeronautics and Space Administration, Marshall Space Flight Center, USA)
Bruno Rudolf (GPCC, Offenbach, Germany)

Tom Smith (NOAA/NESDIS, USA)
Pingping Xie (NOAA/NWS/NCEP/Climate Prediction Center, USA)
Xungang Yin (Cooperative Institute for Climate Studies, Earth System Science Interdisciplinary Center, University of Maryland, USA)

Chapter 4. Future Outlook
Lead Author – Arnold Gruber (Cooperative Institute for Climate Studies, Earth System Science Interdisciplinary Center, University of Maryland, USA)

Manuscript Reviewers
Phillip Arkin (Earth System Science Interdisciplinary Center, University of Maryland, USA)
Christoph Beck (GPCC, Offenbach, Germany)
Elizabeth E. Ebert (Bureau of Meteorology Research Centre, Melbourne, Australia)
Ralph Ferraro (NOAA/NESDIS, USA)
Jürgen Grieser (GPCC, Offenbach, Germany, now at FAO)
George Huffman (SSAI/NASA/GSFC, Greenbelt, USA)
Chris Kidd (School of Geography, Earth and Environmental Sciences, University of Birmingham, UK)
William Rossow (NASA, Goddard Institute for Space Studies, USA)
Tom Smith (NOAA/NESDIS, USA)
Francisco Tapiador (Institute of Environmental Sciences, University of Castilla-La Mancha, Toledo, Spain)

Appendix III. Satellite Missions

Satellite missions and sensors that are used for GPCP precipitation estimation are briefly described hereafter together with a selection of web sites for reference and data collection.

Geostationary Orbit (GEO): visible, near infrared and infrared imagers and sounders

The following table lists the operational geostationary satellites whose data can be accessed by users (situation assessed for November 2005 but is valid for April 2008 as well). An up-to-date list is available at the CGMS website at WMO http://www.wmo.int/web/sat/CGMShome.html.

Sector	Satellites currently in orbit (+mode) P: Pre-operational Op: Operational B: Back-up L: Limited availability	Operator	Location	Launch date
West–Pacific (108° E-180° E)	FY-2B (B)	CHINA/CMA	123.5°E	06/2000
	MTSAT-1R (Op)	JAPAN	140°E	26/02/05
	GOES-9 (L)	USA/NOAA	1555°E	05/95
East–Pacific (180°W-108°W)	GOES-10 (Op)	USA/NOAA	135°W	04/97
West-Atlantic (108°W-36°W)	GOES-12 (Op)	USA/NOAA	75°W	7/ 01
	GOES-11 (B)	USA/NOAA	105°W	05/00
East-Atlantic (36°W-36°E)	Meteosat-6 (B)	EUMETSAT	10°E	11/93
	Meteosat-7 (Op)	EUMETSAT	0°	02/97
	Meteosat-8 (Op)	EUMETSAT	3.4°W	28/08/02
Indian Ocean (36°E-108°E)	Meteosat-5 (Op)	EUMETSAT	63°E	03/91
	FY-2C (Op)	CHINA/CMA	105° E	19/10/2004
	FY-2A (B, L)	CHINA/CMA	86.5° E	06/97

Geostationary Operational Environmental Satellite (GOES). Imager and sounder operated by NOAA. GOES-9 is operating over West Pacific at 155°E, GOES-10 AT 135°e OVER East Pacific, and GOES-12 at 75°W over West Atlantic. GOES-11 is the back at 105°W over West Atlantic.
Description:
GOES-I-M Data Book - http://rsd.gsfc.nasa.gov/goes/text/goes.databook.html.
Official sites and data:
http://www.goes.noaa.gov/
http://www.ssd.noaa.gov/

Meteosat, EUMETSAT's geostationary platform. The Meteosat mission has operated the Meteosat Visible and InfraRed Imager (MVIRI) since 1977. Meteosat 5 is ending its operations over the Indian Ocean at 63°E and Meteosat 7 is now being shifted to substitute it. Meteosat 6 is acting as as the rapid scan satellite at10°E,. From Meteosat 8 (or Meteosat Second Generation 1 – MSG1) the operational mission operates the Spinning Enhanced Visible and InfraRed Imager (SEVIRI) at 0E. Meteosat 9 (MSG2) has been already launched and is presently undergoing tests.
Description:

Schmetz, J., P. Pili, S. Tjemkes, D. Just, J. Kerkmann, S. Rota, and A. Ratier, 2002: An introduction to Meteosat Second Generation (MSG). *Bull. Amer. Meteor. Soc.*, **83**, 977–992.

Official sites and data:
http://www.eumetsat.int/
http://archive.eumetsat.org/en/index.html

Multi-functional Transport SATellite (MTSAT) substituted on 26 February 2005 in orbit the **Geostationary Meteorological Satellite (GMS)**. The last GMS satellite (GMS-5) was substituted into operations by MTSAT-1R. Orbit over the equator at 140°E (West Pacific).
Description, official site and data archive:
http://www.jma.go.jp/jma/jma-eng/satellite/index.html
http://mscweb.kishou.go.jp/index.htm

Feng Yun 2 B (FY-2). Operated by the Chinese Meteorological Agency (CMA). Orbit over the equator at 123.5°E (West Pacific).
Official site:
http://www.cma.gov.cn/.

Low Earth Orbit (LEO): visible, near infrared, infrared and microwave imagers and sounders

The following table (situation assessed for November 2005 but is valid for April 2008 as well) depicts the operational spacecrafts in orbit and is available at the CGMS site at WMO http://www.wmo.int/web/sat/CGMShome.html.

Orbit type (equatorial crossing times)	Satellites in orbit (+operation mode) P=Pre-operational Op=operational B=back-up L=limited availability	Operator	Equator Crossing Time A=Northw D=Southw	Altitude	Launch date
Sun-synchr. "Morning" (6:00 – 12:00) (18:00 – 24:00)	NOAA-17 (Op)	USA/NOAA	10:24 (D)	810 km	6/02
	NOAA-15 (B)	USA/NOAA	05:58 (D)	807 km	05/98
	NOAA-12 (L)	USA/NOAA	04:55 (D)	804 km	05/91
	DMSP-F16 (Op)	USA/NOAA	20 :13 (A)		10/03
	DMSP-F15 (B)	USA/NOAA	20:41 (A)	850 km	12/99
	DMSP-F14 (B)	USA/NOAA	18:36 (A)	852 km	04/97
	Meteor-3M-1(Op)	Russian Federation	9:15 (A)	1020 km	12/01
Sun-synchr. "Afternoon" (12:00 –16:00) (00:00 – 04:00)	NOAA-18 (Op)	USA/NOAA	13:55 (A)	854 km	5/05
	NOAA-16 (B)	USA/NOAA	14:11 (A)	850 km	09/00
	NOAA-14 (B)	USA/NOAA	19:30 (A)	845 km	12/94
Sun-synchr. "Early morning" (4:00 - 6:00) (16:00 – 18:00)	DMSP-F13 (Op)	USA/NOAA	18:33 (A)	850 km	03/95
	FY-1D (Op)	China/CMA	08:20 (D)	866 km	5/02

The main instruments onboard these satellites are:

Special Sensor Microwave Imager (SSM/I) onboard the DMSP satellites
Description:
Hollinger, J. P., R. C. Lo, G. A. Poe, R. Savage, and J. L. Peirce, 1987: Special Sensor Microwave/Imager User's Guide, Naval Research Laboratory, Washington D.C., 177 pp.
http://www.af.mil/factsheets/factsheet.asp?fsID=94.

Special Sensor Microwave Imager/Sounder (SSM/IS) onboard the DMSP satellites.

Advanced Microwave Sounding Unit-A (AMSU-A and B) onboard the NOAA K-L-M satellites.
Description:
http://www2.ncdc.noaa.gov/docs/klm/html/c3/sec3-3.htm
http://www2.ncdc.noaa.gov/docs/klm/html/c3/sec3-4.htm

Advanced Microwave Scanning Radiometer (AMSR) onboard ADEOS-II and **AMSR for EOS (AMSR-E)** onboard EOS Aqua.
Description and data information:
http://sharaku.eorc.jaxa.jp/AMSR/index_e.htm.

A number of other satellites and sensors are worth mentioning for their potential in precipitation area detection and rainrate estimations. They are not directly used for GPCP products, but they might be used for future upcoming versions.

Advanced Very High Resolution Radiometer (AVHRR/2 and 3) onboard NOAA KLM, NOAA 12, 15, 16 and 17.
Description:
http://noaasis.noaa.gov/NOAASIS/ml/avhrr.html

CloudSat recently launched 28 April 2006 by NASA.
Description:
Stephens, G. L., D. G. Vane, R. J. Boain, G. G. Mace, K. Sassen, Z. Wang, A. J. Illingworth, E. J. O'Connor, W. B. Rossow, S. L. Durden, S. D. Miller, R. T. Austin, A. Benedetti, C. Mitrescu, and the CloudSat Science Team, 2002: The CloudSat mission and the A-Train. *Bull. Amer. Meteor. Soc.*, **83**, 1771-1790.
http://cloudsat.atmos.colostate.edu/

Coriolis/WindSat, a joint IPO/DoD/NASA risk reduction demonstration project intended to measure ocean surface *wind speed* and *wind direction* from space using a polarimetric radiometer.
Description:
http://www.nrl.navy.mil/content.php?P=04REVIEW87
http://www.ipo.noaa.gov/Projects/windsat.html
http://code8200.nrl.navy.mil/windsat.html

EUMETSAT Polar System (EPS), the European contribution to the Initial Joint Polar-Orbiting Operational Satellite System (IJPS). In this joint European-US polar satellite system, EUMETSAT will have the operational responsibility for the "morning orbit" with the MetOp satellites.
Description:
http://www.eumetsat.int/idcplg?IdcService=SS_GET_PAGE&nodeId=47&l=en

MODerate Resolution Imaging Spectroradiometer (MODIS) onboard EOS Terra and Aqua.
Description of cloud products and data:

King, M. D., Y. J. Kaufman, W. P. Menzel, and D. Tanré, 1992: Remote sensing of cloud, aerosol, and water vapor properties from the Moderate Resolution Imaging Spectrometer (MODIS). *IEEE Trans. Geosci. Remote Sens.*, **30**, 2-27.

King, M. D., S.-C. Tsay, S. E. Platnick, M. Wang, and K. N. Liou, 1997: Cloud retrieval algorithms for MODIS: optical thickness, effective particle radius, and thermodynamic phase. *ATBD Reference Number: ATBD-MOD-05.*

Menzel, W. P., and K. Strabala, 1997: Cloud top properties and cloud phase - Algorithm Theoretical Basis Document. *ATBD Reference Number: ATBD-MOD-04.*

http://modis.gsfc.nasa.gov/